This is a preprint of: "The geometry of quadratic polynomial differential systems with a finite and an infinite saddle-node (A,B)", Joan Carles Artés, Alex Carlucci Rezende, Regilene D. S. Oliveira, *Internat. J. Bifur. Chaos Appl. Sci. Engrg.*, vol. 24(4), 1450044 (30 pages), 2014.
DOI: [10.1142/S0218127414500448]

THE GEOMETRY OF QUADRATIC POLYNOMIAL DIFFERENTIAL SYSTEMS WITH A FINITE AND AN INFINITE SADDLE–NODE (A, B)

JOAN C. ARTÉS
Departament de Matemàtiques, Universitat Autònoma de Barcelona, 08193 Bellaterra, Barcelona, Spain
E–mail: artes@mat.uab.cat
ALEX C. REZENDE[1] AND REGILENE D. S. OLIVEIRA[2]
Departamento de Matemática, Universidade de São Paulo, 13566–590, São Carlos, São Paulo, Brazil,
E–mail: [1]arezende@icmc.usp.br, [2]regilene@icmc.usp.br

Planar quadratic differential systems occur in many areas of applied mathematics. Although more than one thousand papers have been written on these systems, a complete understanding of this family is still missing. Classical problems, and in particular, Hilbert's 16th problem [Hilbert, 1900, Hilbert, 1902], are still open for this family. Our aim is to make a global study of the family $\overline{QsnSN}$ which is the closure within real quadratic differential systems of the family $QsnSN$ of all such systems which have two semi–elemental saddle–nodes, one finite and one infinite formed by the collision of two infinite singular points. This family can be divided into three different subfamilies, all of them with the finite saddle–node at the origin of the plane with the eigenvectors on the axes and (A) with the infinite saddle–node in the horizontal axis, (B) with the infinite saddle–node in the vertical axis and (C) with the infinite saddle–node in the bisector of the first and third quadrants. These three subfamilies modulo the action of the affine group and time homotheties are three–dimensional (the closure is four–dimensional) and we give their bifurcation diagram with respect to a normal form. In this paper we provide the complete study of the geometry of the first two families, (A) and (B). The bifurcation diagram for the subfamily (A) yields 38 phase portraits for systems in $\overline{QsnSN(A)}$ (29 in $QsnSN(A)$) out of which only 3 have limit cycles and 13 possess graphics. The bifurcation diagram for the subfamily (B) yields 25 phase portraits for systems in $\overline{QsnSN(B)}$ (16 in $QsnSN(B)$) out of which 11 possess graphics. None of the 25 portraits has limit cycles. Case (C) will yield many more phase portraits and will be written separately in a forthcoming new paper. Algebraic invariants are used to construct the bifurcation set. The phase portraits are represented on the Poincaré disk. The bifurcation set of $\overline{QsnSN(A)}$ is formed by algebraic surfaces and one surface whose presence was detected numerically. All points in this surface correspond to connections of separatrices. The bifurcation set of $\overline{QsnSN(B)}$ is formed only by algebraic surfaces.

1. Introduction, brief review of the literature and statement of results

Here we call *quadratic differential systems* or simply *quadratic systems*, differential systems of the form

$$\begin{array}{rcl} \dot{x} & = & p(x,y), \\ \dot{y} & = & q(x,y), \end{array} \tag{1}$$

where p and q are polynomials over $\mathbb{R}$ in x and y such that the $\max(\deg(p),\deg(q)) = 2$. To such a system one can always associate the quadratic vector field

$$X = p\frac{\partial}{\partial x} + q\frac{\partial}{\partial y}, \tag{2}$$

as well as the differential equation

$$qdx - pdy = 0. \tag{3}$$

The class of all quadratic differential systems (or quadratic vector fields) will be denoted by QS.

We can also write system (1) as

$$\begin{array}{rl} \dot{x} & = p_0 + p_1(x,y) + p_2(x,y) = p(x,y), \\ \dot{y} & = q_0 + q_1(x,y) + q_2(x,y) = q(x,y), \end{array} \tag{4}$$

where p_i and q_i are homogeneous polynomials of degree i in (x,y) with real coefficients with $p_2^2+q_2^2 \neq 0$.

Even after hundreds of studies on the topology of real planar quadratic vector fields, it is kind of impossible to outline a complete characterization of their phase portraits, and attempting to topologically classify them is a quite complex task. This family of systems depends on twelve parameters, but due to the action of the group G of real affine transformations and time homotheties, the class ultimately depends on five parameters, but this is still a large number.

This paper is aimed at studying the class $\overline{QsnSN}$ which is the closure within real quadratic real differential systems of the family $QsnSN$ of all such systems which possess a finite saddle–node $\overline{sn}_{(2)}$ and an infinite saddle–node of type $\binom{0}{2}SN$ obtained by the collision of an infinite saddle with an infinite node. The finite saddle–node is a semi–elemental point whose neighborhood is formed by the union of two hyperbolic sectors and one parabolic sector. By a semi–elemental point we understand a point with zero determinant of its Jacobian, but only one eigenvalue zero. These points are known in classical literature as semi–elementary, but we use the term semi–elemental introduced in [Artés *et al.*, 2012] as part of a set of new definitions more deeply related to the geometry of the singular points, their multiplicities and, especially, their Jacobian matrices. We observe that there is another type of infinite saddle–node denoted by $\overline{\binom{1}{1}}SN$ which is given by the collision of a finite antisaddle (respectively, finite saddle) with an infinite saddle (respectively, infinite node) and which will appear in some of the phase portraits.

The condition of having a finite saddle–node of all the systems in $QsnSN$ implies that these systems may have up to two other finite points.

For a general framework of the study of the class of all quadratic differential systems we refer to the article of Roussarie and Schlomiuk [Roussarie & Schlomiuk, 2002].

In this study we follow the pattern set out in [Artés *et al.*, 2006]. As much as possible we shall try to avoid repeating technical sections which are the same for both papers, referring to the paper mentioned just above, for more complete information.

This family can be divided into three different subfamilies, all of them with the finite saddle–node at the origin of the plane with the eigenvectors on the axes and (A) with the infinite saddle–node in the horizontal axis, (B) with the infinite saddle–node in the vertical axis and (C) with the infinite saddle–node in the bisector of the first and third quadrants.

In this article we give a partition of the classes $\overline{QsnSN(A)}$ and $\overline{QsnSN(B)}$. The first class $\overline{QsnSN(A)}$ is partitioned into 85 parts: 23 three–dimensional ones, 37 two–dimensional ones, 20 one–dimensional ones and 5 points. This partition is obtained by considering all the bifurcation surfaces of singularities, one related to the presence of another invariant straight rather than the one stated in statement *(a)* of Theorem 1.1 and one related to connections of separatrices, modulo "islands" (see Sec. 8). The second class $\overline{QsnSN(B)}$ is partitioned into 43 parts: 9 three–dimensional ones, 18 two–dimensional ones, 12 one–dimensional ones and 4 points, which are all delimited by algebraic bifurcation surfaces.

A *graphic* as defined in [Dumortier *et al.*, 1994] is formed by a finite sequence of singular points

$r_1, r_2, \ldots, r_n$ (with possible repetitions) and non–trivial connecting orbits γ_i for $i = 1, \ldots, n$ such that γ_i has r_i as α–limit set and r_{i+1} as ω–limit set for $i < n$ and γ_n has r_n as α–limit set and r_1 as ω–limit set. Also normal orientations n_j of the non–trivial orbits must be coherent in the sense that if γ_{j-1} has left–hand orientation then so does γ_j. A *polycycle* is a graphic which has a Poincaré return map.

A *degenerate graphic* is a graphic where it is also allowed that one or several (even all) connecting orbits γ_i can be formed by an infinite number of singular points. For more details, see [Dumortier *et al.*, 1994].

Theorem 1.1. *There exist 38 topologically distinct phase portraits for the quadratic vector fields having a finite saddle–node* $\overline{sn}_{(2)}$ *and an infinite saddle–node of type* $\binom{0}{2}SN$ *located in the direction defined by the eigenvector with null eigenvalue (class* $\overline{QsnSN(A)}$*). All these phase portraits are shown in Figs. 1 and 2. Moreover, the following statements hold:*

(a) The manifold defined by the eigenvector with null eigenvalue is always an invariant straight line under the flow;

(b) There exist three phase portraits with limit cycles, and they are in the regions V_{11}^5, V_{14}^7 *and* $1S_2^{11}$*;*

(c) There exist three phase portraits with non-degenerate graphics, and they are in the regions $4S_4^{19}$, $7S_1^{23}$ *and* $1.4L_1^{28}$*;*

(d) There exist ten phase portraits with degenerate graphics, and they are in the regions $9S_1^{24}$, $9S_2^{25}$, $1.2L_2^{27}$, $1.9L_1^{29}$, $5.9L_1^{33}$, $8.9L_1^{34}$, P_1^{35}, P_3^{36}, P_4^{37} *and* P_5^{38}*;*

(e) Any phase portrait of this family can bifurcate from P_1^{35} *of Fig. 2;*

(f) There exist 29 topologically distinct phase portraits in $QsnSN(A)$*.*

Theorem 1.2. *There exist 25 topologically distinct phase portraits for the quadratic vector fields having a finite saddle–node* $\overline{sn}_{(2)}$ *and an infinite saddle–node of type* $\binom{0}{2}SN$ *located in the direction defined by the eigenvector with non–null eigenvalue (class* $\overline{QsnSN(B)}$*). All these phase portraits are shown in Fig. 3. Moreover, the following statements hold:*

(a) The manifold defined by the eigenvector with non–null eigenvalue is always an invariant straight line under the flow;

(b) There exist four phase portraits with non-degenerate graphic, and they are in the regions $1S_4^9$, $4S_1^{10}$, $1.4L_2^{16}$ *and* $1.5L_1^{17}$*;*

(c) There exist seven phase portraits with degenerate graphics, and they are in the regions $1.4L_1^{15}$, $1.9L_1^{18}$, $4.9L_1^{19}$, P_1^{22}, P_2^{23}, P_3^{24} *and* P_5^{25}*;*

(d) There exists one phase portrait with a center, and it is in the region $4S_1^{10}$*;*

(e) There exists one phase portrait with an integrable saddle, and it is in the region $4S_2^1$*.*

(f) Any phase portrait of this family can bifurcate from P_1^{22} *of Fig. 3;*

(g) There exist 16 topologically distinct phase portraits in $QsnSN(B)$*.*

Corollary 1.3. *The phase portrait* P_3^{36} *from family* $\overline{QsnSN(A)}$ *in Fig. 2 is equivalent to the phase portrait* P_2^{23} *from family* $\overline{QsnSN(B)}$ *in Fig. 3. Furthermore, the phase portrait* $1.2L_2^{27}$ *from family* $\overline{QsnSN(A)}$ *in Fig. 2 is equivalent to the phase portrait* $1.4L_1^{15}$ *from family* $\overline{QsnSN(B)}$ *in Fig. 3.*

For the class $QsnSN(A)$, from its 29 topologically different phase portraits, 9 occur in 3–dimensional parts, 14 in 2–dimensional parts, 5 in 1–dimensional parts and 1 occur in a single 0–dimensional part, and for the class $QsnSN(B)$, from its 16 topologically different phase portraits, 5 occur in 3–dimensional parts, 7 in 2–dimensional parts, 3 in 1–dimensional parts and 1 occur in a single 0–dimensional part.

In Figs. 1, 2 and 3 we have denoted all the singular points with a small disk. We have plotted with wide curves the separatrices and we have added some orbits drawn on the picture with thinner lines to avoid confusion in some required cases.

Remark 1.4. We label the phase portraits according to the parts of the bifurcation diagram where

they occur. These labels could be different for two topologically equivalent phase portraits occurring in distinct parts. Some of the phase portraits in 3–dimensional parts also occur in some 2–dimensional parts bordering these 3–dimensional parts. An example occurs when a node turns into a focus. An analogous situation happens for phase portraits in 2–dimensional (respectively, 1–dimensional) parts, coinciding with a phase portrait on 1–dimensional (respectively, 0–dimensional) part situated on the border of it.

The work is organized as follows. In Sec. 2 we describe the normal form for the families of systems having a finite saddle–node and an infinite saddle–node of type $\overline{\binom{0}{2}}SN$ in both horizontal and vertical axes.

For the study of real planar polynomial vector fields two compactifications can be used. In Sec. 3 we describe very briefly the Poincaré compactification on the 2–dimensional sphere.

In Sec. 4 we list some very basic properties of general quadratic systems needed in this study.

In Sec. 5 we mention some algebraic and geometric concepts that were introduced in [Schlomiuk *et al.*, 2001, Llibre *et al.*, 2004] involving intersection numbers, zero–cycles, divisors, T–comitant and invariant polynomials for quadratic systems as used by the Sibirskii school. We refer the reader directly to [Artés *et al.*, 2006] where these concepts are widely explained.

We construct in Secs. 6 and 7 the algebraic bifurcation surfaces of singularities for the classes $\overline{QsnSN(A)}$ and $\overline{QsnSN(B)}$, respectively.

In Sec. 8 we comment about the possible existence of "islands" in the bifurcation diagram.

In Sec. 9 we introduce a global invariant denoted by $\mathcal{I}$, which classifies completely, up to topological equivalence, the phase portraits we have obtained for the systems in the classes $\overline{QsnSN(A)}$ and $\overline{QsnSN(B)}$. Theorems 9.11 and 9.12 show clearly that they are uniquely determined (up to topological equivalence) by the values of the invariant $\mathcal{I}$.

Remark 1.5. It is worth mentioning that a third subclass $\overline{QsnSN(C)}$ of $\overline{QsnSN}$ must be considered. This subclass consists of planar quadratic systems with a finite saddle–node $\overline{sn}_{(2)}$ also situated at the origin (as we do in this work) and an infinite saddle–node of type $\overline{\binom{0}{2}}SN$ in the bisector of the first and third quadrants and it is currently being studied.

In [Artés *et al.*, 1998] the authors classified all the structurally stable quadratic planar systems modulo limit cycles, also known as the codimension–zero quadratic systems (roughly speaking, those systems whose all singularities, finite and infinite, are simple, with no separatrix connection, and where any nest of limit cycles is identified with the focus inside of them, with the stability of the last limit cycle) by proving the existence of 44 topologically different phase portraits for these systems. The natural continuation in this idea is the classification of the structurally unstable quadratic systems of codimension–one, i.e. those systems which have one and only one of the following simplest structurally unstable objects: a saddle–node of multiplicity two (finite or infinite), a separatrix from one saddle point to another, and a separatrix forming a homoclinic loop with its divergence non–zero. This study is already in progress [Artés & Llibre, 2013], all topological possibilities have already been found, some of them have already been proved impossible and many representatives have been located, but there remain some cases without a candidate. One way to obtain codimension–one phase portraits is considering perturbations of known phase portraits of quadratic systems of higher degree of degeneracy. These perturbations would decrease the codimension of the system and we may find a representative for a topological equivalence class in the family of the codimension–one systems and add it to the existing classification.

In order to contribute to this classification, we studied some families of quadratic systems of higher degree of degeneracy, e.g. systems with a weak focus of second order, see [Artés *et al.*, 2006], and with a finite semi–elemental triple node, see [Artés *et al.*, 2013]. In this last paper, the authors show that, after a quadratic perturbation in the phase portrait V_{11}, the semi–elemental triple node is split into a node and a saddle–node and the new phase portrait is topologically equivalent to one of the topologically possible phase portraits of codimension one, expected to exist.

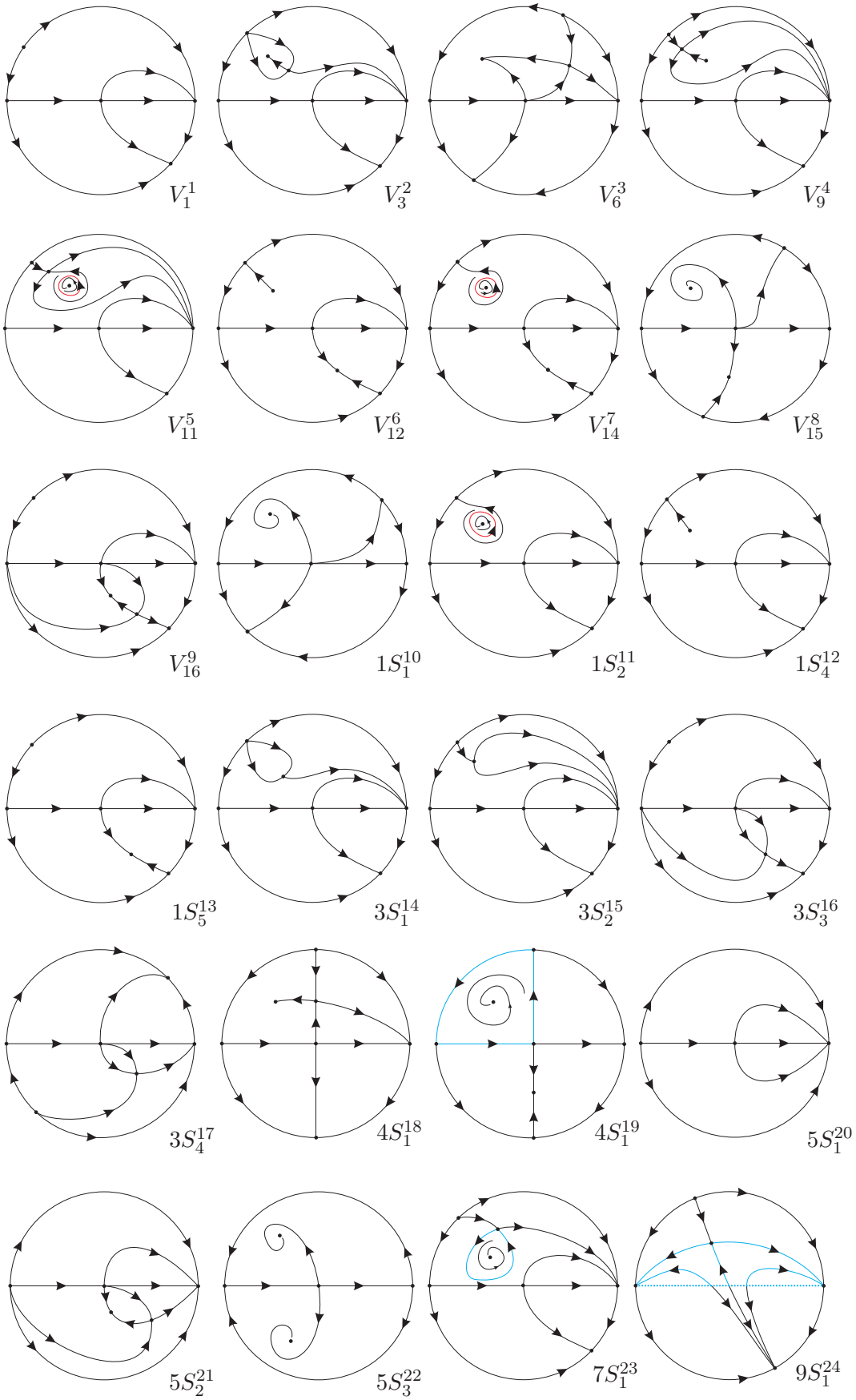

Fig. 1. Phase portraits for quadratic vector fields with a finite saddle–node $\overline{sn}_{(2)}$ and an infinite saddle–node of type $\overline{\binom{0}{2}}SN$ in the horizontal axis.

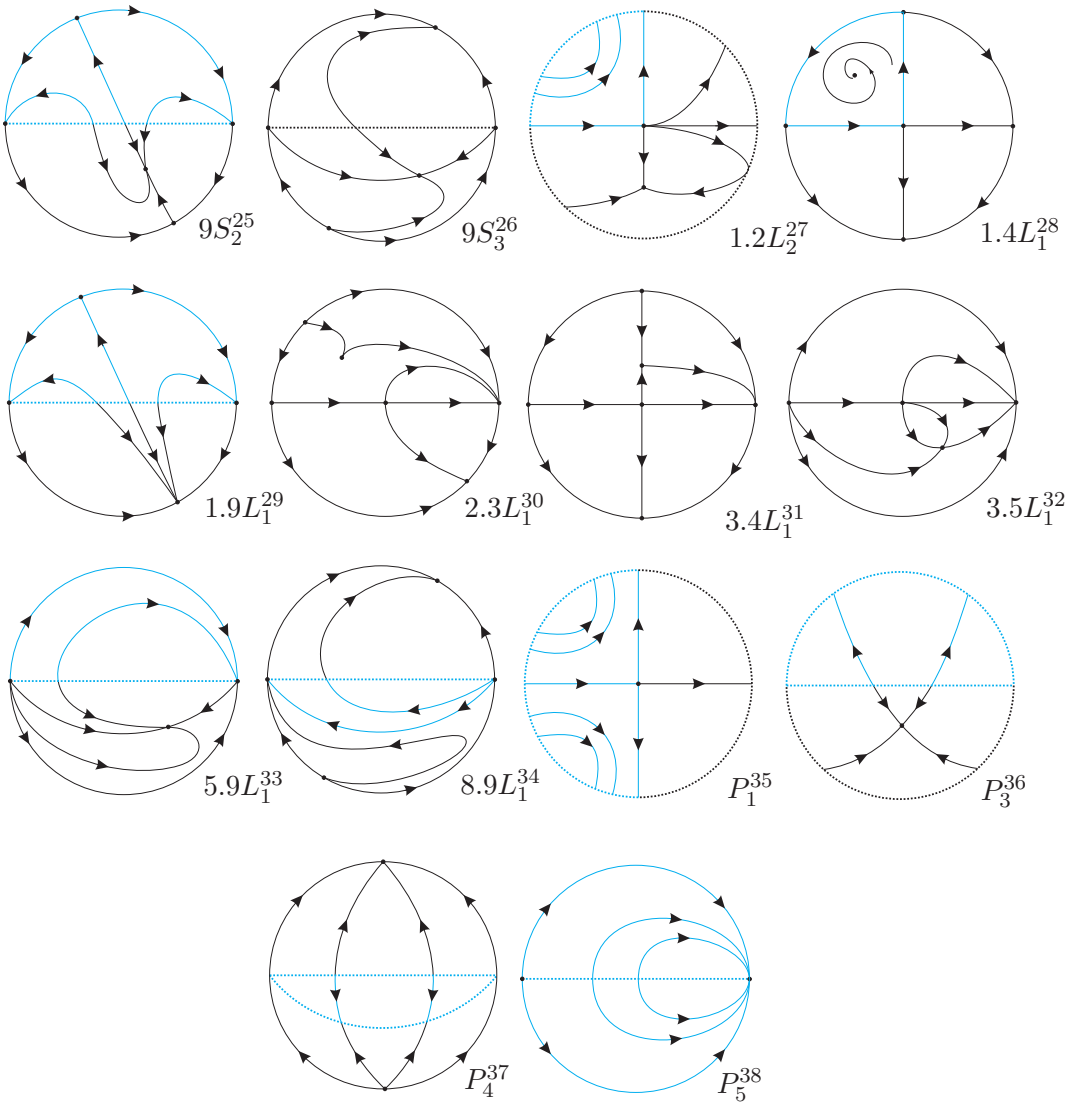

Fig. 2. Continuation of Fig. 1.

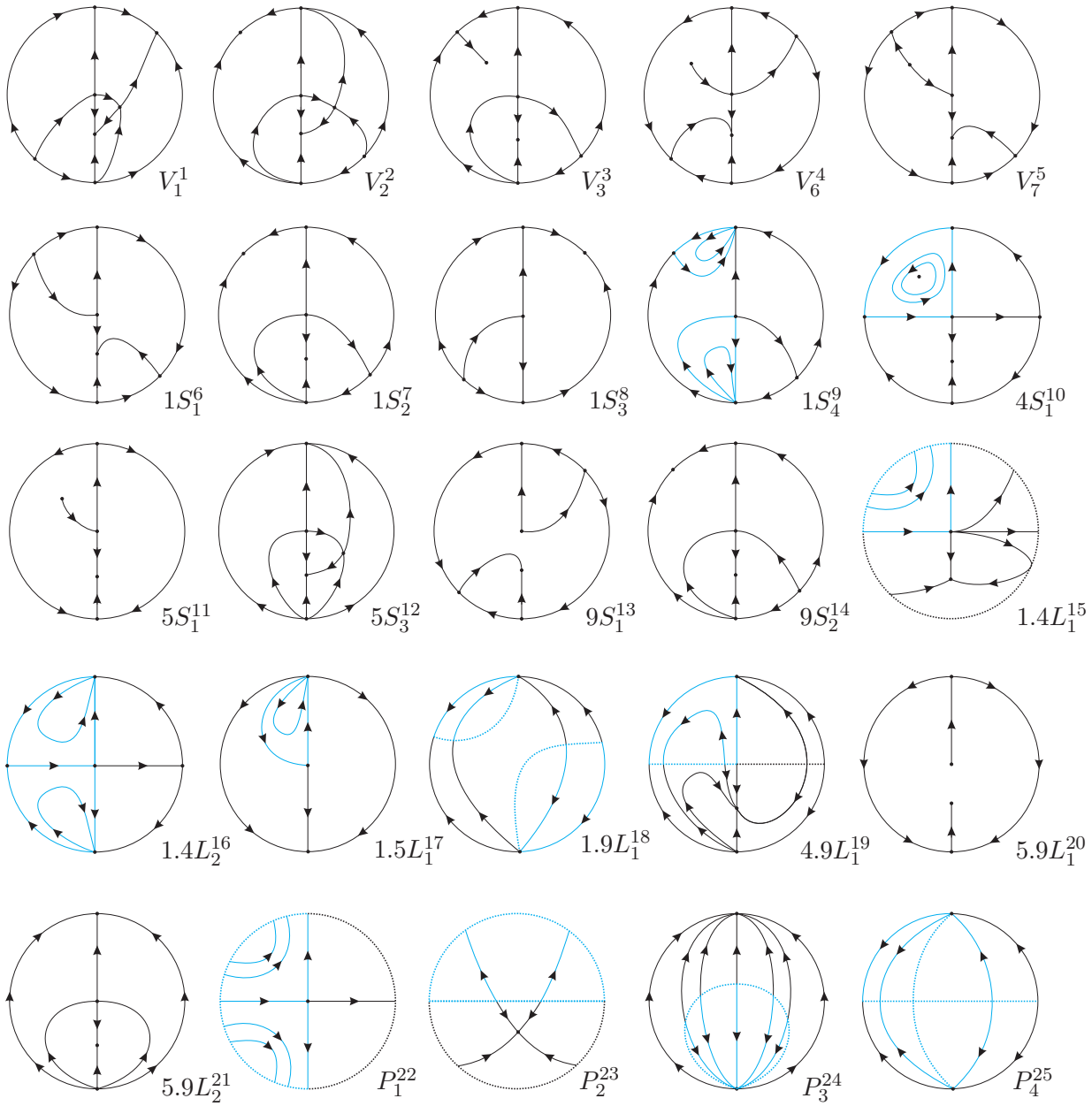

Fig. 3. Phase portraits for quadratic vector fields with a finite saddle–node $\overline{sn}_{(2)}$ and an infinite saddle–node of type $\overline{\binom{0}{2}}SN$ in the vertical axis.

The present study is part of this attempt of classifying all the codimension–one quadratic systems. We propose the study of a whole family of quadratic systems having two semi–elemental saddle–nodes, one finite and one infinite formed by the collision of two infinite singular points. Both subfamilies reported here will not bifurcate to any of the codimension–one systems still missing, but in the subfamily $\overline{QsnSN(C)}$ will appear some new examples due to the highly rich bifurcation diagram, richer than anything we encountered before.

2. Quadratic vector fields with a finite saddle–node $\overline{sn}_{(2)}$ and an infinite saddle–node of type $\binom{\overline{0}}{2}SN$

A singular point r of a planar vector field X in $\mathbb{R}^2$ is *semi–elemental* if the determinant of the matrix of its linear part, $DX(r)$, is zero, but its trace is different from zero.

The following result characterizes the local phase portrait at a semi–elemental singular point.

Proposition 2.1. *[Andronov* et al.*, 1973, Dumortier* et al.*, 2006] Let $r = (0,0)$ be an isolated singular point of the vector field X given by*

$$\begin{aligned} \dot{x} &= M(x,y), \\ \dot{y} &= y + N(x,y), \end{aligned} \tag{5}$$

where M and N are analytic in a neighborhood of the origin starting with at least degree 2 in the variables x and y. Let $y = f(x)$ be the solution of the equation $y + N(x,y) = 0$ in a neighborhood of the point $r = (0,0)$, and suppose that the function $g(x) = M(x, f(x))$ has the expression $g(x) = ax^\alpha + o(x^\alpha)$, where $\alpha \geq 2$ and $a \neq 0$. So, when α is odd, then $r = (0,0)$ is either an unstable multiple node, or a multiple saddle, depending if $a > 0$, or $a < 0$, respectively. In the case of the multiple saddle, the separatrices are tangent to the x–axis. If α is even, $r = (0,0)$ is a multiple saddle–node, i.e. the singular point is formed by the union of two hyperbolic sectors with one parabolic sector. The stable separatrix is tangent to the positive (respectively, negative) x–axis at $r = (0,0)$ according to $a < 0$ (respectively, $a > 0$). The two unstable separatrices are tangent to the y–axis at $r = (0,0)$.

In the particular case where M and N are real quadratic polynomials in the variables x and y, a quadratic system with a semi–elemental singular point at the origin can always be written into the form

$$\begin{aligned} \dot{x} &= gx^2 + 2hxy + ky^2, \\ \dot{y} &= y + \ell x^2 + 2mxy + ny^2. \end{aligned} \tag{6}$$

By Proposition 2.1, if $g \neq 0$, then we have a double saddle–node $\overline{sn}_{(2)}$, using the notation introduced in [Artés *et al.*, 2012].

In the normal form above, we consider the coefficient of the terms xy in both equations factored by 2 in order to make easier the calculations of the algebraic invariants we shall compute later.

We note that in the normal form (6) we already have a semi–elemental point at the origin and its eigenvectors are $(1,0)$ and $(0,1)$ which condition the possible positions of the infinite singular points.

We suppose that there exists a $\binom{\overline{0}}{2}SN$ at some point at infinity. If this point is different from either $[1:0:0]$ of the local chart U_1, or $[0:1:0]$ of the local chart U_2, after a reparametrization of the type $(x,y) \to (x, \alpha y)$, $\alpha \in \mathbb{R}$, this point can be replaced at $[1:1:0]$ of the local chart U_1, that is, at the bisector of the first and third quadrants. However, if $\binom{\overline{0}}{2}SN$ is at $[1:0:0]$ or $[0:1:0]$, we cannot apply this change of coordinates and it requires an independent study for each one of the cases, which are not equivalent due to the position of the infinite saddle–node with respect to the eigenvectors of the finite saddle–node. See Sec. 3 for the notation.

2.1. The normal form for the subclass $\overline{QsnSN(A)}$

The following result states the normal form for systems in $\overline{QsnSN(A)}$.

Proposition 2.2. *Every system with a finite semi–elemental double saddle–node $\overline{sn}_{(2)}$ and an infinite saddle–node of type $\binom{\overline{0}}{2}SN$ located in the direction defined by the eigenvector with null eigenvalue can be brought via affine transformations and time rescaling to the following normal form*

$$\begin{aligned} \dot{x} &= gx^2 + 2hxy + ky^2, \\ \dot{y} &= y + gxy + ny^2, \end{aligned} \tag{7}$$

where g, h, k and n are real parameters and $g \neq 0$.

Proof. We start with system (6). This system already has a finite semi–elemental double saddle–node at the origin (then $g \neq 0$) with its eigenvectors in the direction of the axes. The first step is to place the point $\binom{0}{2}SN$ at the origin of the local chart U_1 with coordinates (w, z). For that, we must guarantee that the origin is a singularity of the flow in U_1,

$$\dot{w} = \ell + (-g + 2m)w + (-2h + n)w^2 - kw^3 + wz,$$
$$\dot{z} = (-g - 2hw - kw^2)z.$$

Then, we set $\ell = 0$ and, by analyzing the Jacobian of the former expression, we set $m = g/2$ in order to have the eigenvalue associated to the eigenvector on $z = 0$ being null and obtain the normal form (7). ∎

In order to consider the closure of the family $QsnSN(A)$, it is necessary to study the case when $g = 0$, which will be discussed later.

Remark 2.3. We note that $\{y = 0\}$ is an invariant straight line under the flow of (7).

Systems (7) depend on the parameter $\lambda = (g, h, k, n) \in \mathbb{R}^4$. We consider systems (7) which are nonlinear, i.e. $\lambda = (g, h, k, n) \neq 0$. In this case, system (7) can be rescaled $(x \mapsto x/g)$ and the parameter space is actually the real projective plane $\mathbb{RP}^3$, and not $\mathbb{R}^4$. The 3–dimensional projective space $\mathbb{RP}^3$ can be viewed as the quotient space $\mathbb{S}^3/_\sim$ of $\mathbb{S}^3$ by the equivalence relation: (g, h, k, n) is equivalent to itself or to $(-g, -h, -k, -n)$. So, our parameter is $[\lambda] = [g : h : k : n] \in \mathbb{RP}^3 = \mathbb{S}^3/_\sim$. Rescaling the time, it suffices to consider the points $[g : h : k : n]$ in this quotient with $h \geq 0$. Due to the symmetry $(x, y, t) \mapsto (-x, -y, t)$ we have $(g, h, k, n) \mapsto (-g, -h, -k, -n)$. Indeed, after applying the symmetry $(x, y, t) \mapsto (-x, -y, t)$ we obtain the system

$$\dot{x} = -gx^2 - 2hxy - ky^2,$$
$$\dot{y} = y - gxy - ny^2.$$

This implies that it is sufficient to consider only $g \geq 0$. Since $g^2 + h^2 + k^2 + n^2 = 1$, then $g = \sqrt{1 - (h^2 + k^2 + n^2)}$, where $0 \leq h^2 + k^2 + n^2 \leq 1$.

We can therefore view the parameter space as a half–ball $\mathcal{B} = \{(h, k, n) \in \mathbb{R}^3;\ h^2 + k^2 + n^2 \leq 1,\ h \geq 0\}$ with base $h = 0$ and where on the equator two opposite points are identified. When $h = 0$, we identify the point $[g : 0 : k : n] \in \mathbb{RP}^3$ with $[g : k : n] \in \mathbb{RP}^2$. So, the base of the half–ball $\mathcal{B}$ $(h = 0)$ can be identified with $\mathbb{RP}^2$, which can be viewed as a disk with two opposite points on the circumference (the equator) identified (see Fig. 4).

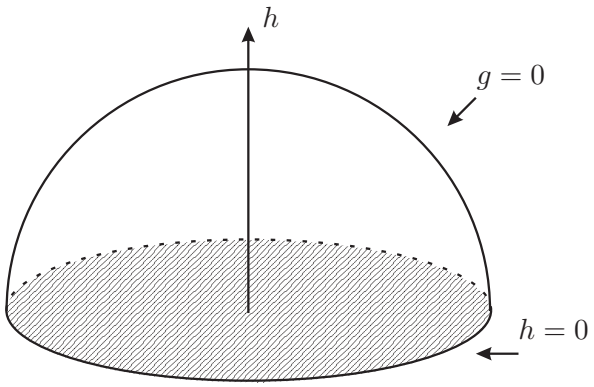

Fig. 4. The parameter space.

For $g \neq 0$, we get the affine chart:

$$\mathbb{RP}^3 \setminus \{g = 0\} \leftrightarrow \mathbb{R}^3$$
$$[g : h : k : n] \mapsto (\frac{h}{g}, \frac{k}{g}, \frac{n}{g}) = (\overline{h}, \overline{k}, \overline{n})$$
$$[1 : \overline{h} : \overline{k} : \overline{n}] \mapsto (\overline{h}, \overline{k}, \overline{n}).$$

The plane $g = 0$ in $\mathbb{RP}^3$ corresponds to the equation $h^2+k^2+n^2 = 1$ (the full sphere $\mathbb{S}^2$) and the line $g = h = 0$ in $\mathbb{RP}^3$ corresponds to the equation $k^2 + n^2 = 1$ (the equator $h = 0$ of $\mathbb{S}^2$). However, because of symmetry, we only need half sphere and half equator, respectively.

We now consider planes in $\mathbb{R}^3$ of the form $\overline{h} = h_0$, where h_0 is a constant. The projective completion of such a plane in $\mathbb{RP}^3$ has the equation $h - h_0 g = 0$. So we see how the slices $\overline{h} = h_0$ need to be completed in the ball (see Fig. 5). We note that when $g = 0$ necessarily we must have $h = 0$ on such a slice, and thus the completion of the image of the plane $\overline{h} = h_0$, when visualized in $\mathbb{S}^3$, must include the equator.

The specific equations of the correspondence of the points in the plane $\overline{h} = h_0$ of $\mathbb{R}^3$ (h_0 a constant) onto points in the interior of $\mathbb{S}^2$ ($\mathcal{B} = \{(h, k, n) \in$

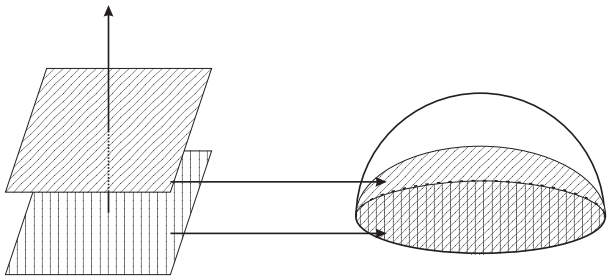

Fig. 5. Correspondence between planes and ellipsoides.

$\mathbb{R}^3$; $h^2+k^2+n^2<1\}$) follows from the bijection:

$$\mathbb{R}^3 \leftrightarrow \mathcal{B}$$
$$(\overline{h},\overline{k},\overline{n}) \leftrightarrow \left(\frac{\overline{h}}{c},\frac{\overline{k}}{c},\frac{\overline{n}}{c}\right)$$

with $c=\sqrt{\overline{h}^2+\overline{k}^2+\overline{n}^2+1}$. That is, for each plane $\overline{h}=$ constant in $\mathbb{R}^3$, there corresponds an ellipsoid $h^2(1+h_0)^2/h_0^2+k^2+n^2=1$ (see Fig. 5).

The set defined by $g=0$ and $h=1$ corresponds to the open half sphere, while $g=0=h$ is the equator of the ball.

In what follows we would have to make a similar study of the geometry of the different surfaces (singularities, intersections, suprema) involved in the bifurcation diagram as it has been done in [Artés *et al.*, 2006] or [Artés *et al.*, 2013]. The conclusion of such a study is that this bifurcation diagram has only one singular slice, $h=0$, plus a symmetry $h\mapsto -h$, so that the only needed slices to be studied are $h=0$ (singular) and $h=1$ (generic). However, there is a much shorter and easier way to detect the same phenomenon and this comes from the next result.

Proposition 2.4. *By a rescaling in the variables, we may assume $h=0$ or $h=1$ in the normal form* (7).

Proof. If $h\neq 0$, we consider the rescaling in the variables given by $(x,y)\mapsto(x,y/h)$ and obtain

$$\begin{aligned}\dot{x} &= gx^2+2xy+\tfrac{k}{h^2}y^2,\\ \dot{y} &= y+gxy+\tfrac{n}{h}y^2.\end{aligned}$$

By recalling the coefficients $k/h^2\mapsto k$ and $n/h\mapsto n$, we obtain system (7) with $h=1$. Moreover, we must also consider the case when $h=0$. ■

2.2. The normal form for the subclass $\overline{QsnSN(B)}$

The following result gives the normal form for systems in $\overline{QsnSN(B)}$.

Proposition 2.5. *Every system with a finite semi–elemental double saddle–node $\overline{sn}_{(2)}$ and an infinite saddle–node of type $\binom{0}{2}SN$ located in the direction defined by the eigenvector with non-null eigenvalue can be brought via affine transformations and time rescaling to the following normal form*

$$\begin{aligned}\dot{x} &= gx^2+2hxy,\\ \dot{y} &= y+\ell x^2+2mxy+2hy^2,\end{aligned} \tag{8}$$

where g, h, ℓ and m are real parameters and $g\neq 0$.

Proof. Analogously to Proposition 2.2, we start with system (6), but now we want to place the point $\binom{0}{2}SN$ at the origin of the local chart U_2. By following the same steps, we set $k=0$, $n=2h$ and we obtain the form (8). ■

For this family, we also study the case when $g=0$ in order to consider the closure of the set $QsnSN(B)$.

Remark 2.6. We note that $\{x=0\}$ is an invariant straight line under the flow of (8).

We construct the parameter space for systems (8) in the same way it was constructed for systems (7), but now with respect to the parameter $[\lambda]=[g:h:\ell:m]\in\mathbb{RP}^3$.

Analogously to the previous family, the bifurcation diagram for this family in $\mathbb{R}^3$ shows only one singular slice, $h=0$, and a symmetry $h\mapsto -h$. Then, only one generic slice needs to be taken into consideration, and we choose $h=1$, and this also can be proved in a much easier way with a transformation similar to the previous case as it can be seen in the next result.

Proposition 2.7. *By a rescaling in the variables, we may assume $h=0$ or $h=1$ in the normal form* (8).

Proof. If $h\neq 0$, we consider the rescaling in the

variables given by $(x, y) \mapsto (x, y/h)$ and obtain

$$\begin{aligned} \dot{x} &= gx^2 + 2xy, \\ \dot{y} &= y + \ell h x^2 + 2mxy + 2y^2. \end{aligned}$$

By recalling the coefficient $\ell h \mapsto \ell$, we obtain system (8) with $h = 1$. Moreover, we must also consider the case when $h = 0$. ■

3. The Poincaré compactification and the complex (real) foliation with singularities on $\mathbb{CP}^2$ ($\mathbb{RP}^2$)

A real planar polynomial vector field ξ can be compactified on the sphere as follows. Consider the x, y plane as being the plane $Z = 1$ in the space $\mathbb{R}^3$ with coordinates X, Y, Z. The central projection of the vector field ξ on the sphere of radius one yields a diffeomorphic vector field on the upper hemisphere and also another vector field on the lower hemisphere. There exists (for a proof see [Gonzales, 1969]) an analytic vector field $cp(\xi)$ on the whole sphere such that its restriction on the upper hemisphere has the same phase curves as the one constructed above from the polynomial vector field. The projection of the closed northern hemisphere H^+ of $\mathbb{S}^2$ on $Z = 0$ under $(X, Y, Z) \to (X, Y)$ is called *the Poincaré disk*. A singular point q of $cp(\xi)$ is called an *infinite* (respectively, *finite*) singular point if $q \in \mathbb{S}^1$, the equator (respectively, $q \in \mathbb{S}^2 \setminus \mathbb{S}^1$). By the *Poincaré compactification of a polynomial vector field* we mean the vector field $cp(\xi)$ restricted to the upper hemisphere completed with the equator.

Ideas in the remaining part of this section go back to Darboux's work [Darboux, 1878]. Let $p(x, y)$ and $q(x, y)$ be polynomials with real coefficients. For the vector field

$$p\frac{\partial}{\partial x} + q\frac{\partial}{\partial y}, \tag{9}$$

or equivalently for the differential system

$$\dot{x} = p(x, y), \qquad \dot{y} = q(x, y), \tag{10}$$

we consider the associated differential 1–form $\omega_1 = q(x, y)dx - p(x, y)dy$, and the differential equation

$$\omega_1 = 0\ . \tag{11}$$

Clearly, equation (11) defines a foliation with singularities on $\mathbb{C}^2$. The affine plane $\mathbb{C}^2$ is compactified on the complex projective space $\mathbb{CP}^2 = (\mathbb{C}^3 \setminus \{0\})/\sim$, where $(X, Y, Z) \sim (X', Y', Z')$ if and only if $(X, Y, Z) = \lambda(X', Y', Z')$ for some complex $\lambda \neq 0$. The equivalence class of (X, Y, Z) will be denoted by $[X : Y : Z]$.

The foliation with singularities defined by equation (11) on $\mathbb{C}^2$ can be extended to a foliation with singularities on $\mathbb{CP}^2$ and the 1–form ω_1 can be extended to a meromorphic 1–form ω on $\mathbb{CP}^2$ which yields an equation $\omega = 0$, i.e.

$$A(X, Y, Z)dX + B(X, Y, Z)dY + C(X, Y, Z)dZ = 0, \tag{12}$$

whose coefficients A, B, C are homogeneous polynomials of the same degree and satisfy the relation:

$$A(X, Y, Z)X + B(X, Y, Z)Y + C(X, Y, Z)Z = 0, \tag{13}$$

Indeed, consider the map $i : \mathbb{C}^3 \setminus \{Z = 0\} \to \mathbb{C}^2$, given by $i(X, Y, Z) = (X/Z, Y/Z) = (x, y)$ and suppose that $\max\{\deg(p), \deg(q)\} = m > 0$. Since $x = X/Z$ and $y = Y/Z$ we have:

$$dx = (ZdX - XdZ)/Z^2, \quad dy = (ZdY - YdZ)/Z^2,$$

the pull–back form $i^*(\omega_1)$ has poles at $Z = 0$ and yields the equation

$$\begin{aligned} i^*(\omega_1) =& q(X/Z, Y/Z)(ZdX - XdZ)/Z^2 \\ & - p(X/Z, Y/Z)(ZdY - YdZ)/Z^2 = 0. \end{aligned}$$

Then, the 1–form $\omega = Z^{m+2} i^*(\omega_1)$ in $\mathbb{C}^3 \setminus \{Z \neq 0\}$ has homogeneous polynomial coefficients of degree $m + 1$, and for $Z = 0$ the equations $\omega = 0$ and $i^*(\omega_1) = 0$ have the same solutions. Therefore, the differential equation $\omega = 0$ can be written as (12), where

$$\begin{aligned} A(X, Y, Z) =& ZQ(X, Y, Z) = Z^{m+1} q(X/Z, Y/Z), \\ B(X, Y, Z) =& -ZP(X, Y, Z) = -Z^{m+1} p(X/Z, Y/Z), \\ C(X, Y, Z) =& YP(X, Y, Z) - XQ(X, Y, Z). \end{aligned} \tag{14}$$

Clearly A, B and C are homogeneous polynomials of degree $m + 1$ satisfying (13).

In particular, for our quadratic systems (7), A, B and C take the following forms

$$\begin{aligned} A(X, Y, Z) =& YZ(gX + nY + Z) \\ B(X, Y, Z) =& -(gX^2 + 2hXY + kY^2)Z, \\ C(X, Y, Z) =& Y(2hXY - nXY + kY^2 - XZ). \end{aligned} \tag{15}$$

and for our quadratic systems (8), A, B and C take the following forms

$$\begin{aligned} A(X,Y,Z) =& Z(\ell X^2 + 2mXY + 2hY^2 + YZ),\\ B(X,Y,Z) =& -X(gX + 2hY)Z,\\ C(X,Y,Z) =& X(-\ell X^2 + gXY - 2mXY - YZ). \end{aligned} \tag{16}$$

We note that the straight line $Z = 0$ is always an algebraic invariant curve of this foliation and that its singular points are the solutions of the system: $A(X,Y,Z) = B(X,Y,Z) = C(X,Y,Z) = 0$. We note also that $C(X,Y,Z)$ does not depend on h.

To study the foliation with singularities defined by the differential equation (12) subject to (13) with A, B, C satisfying the above conditions in the neighborhood of the line $Z = 0$, we consider the two charts of $\mathbb{CP}^2$: $(u,z) = (Y/X, Z/X)$, $X \neq 0$, and $(v,w) = (X/Y, Z/Y)$, $Y \neq 0$, covering this line. We note that in the intersection of the charts $(x,y) = (X/Z, Y/Z)$ and (u,z) (respectively, (v,w)) we have the change of coordinates $x = 1/z$, $y = u/z$ (respectively, $x = v/w$, $y = 1/w$). Except for the point $[0:1:0]$ or the point $[1:0:0]$, the foliation defined by equations (12),(13) with A, B, C as in (14) yields in the neighborhood of the line $Z = 0$ the foliations associated with the systems

$$\begin{aligned} \dot{u} =& uP(1,u,z) - Q(1,u,z) = C(1,u,z),\\ \dot{z} =& zP(1,u,z), \end{aligned} \tag{17}$$

or

$$\begin{aligned} \dot{v} =& vQ(v,1,w) - P(v,1,w) = -C(v,1,w),\\ \dot{w} =& wP(v,1,w). \end{aligned} \tag{18}$$

In a similar way we can associate a real foliation with singularities on $\mathbb{RP}^2$ to a real planar polynomial vector field.

4. A few basic properties of quadratic systems relevant for this study

We list below results which play a role in the study of the global phase portraits of the real planar quadratic systems (1) having a semi–elemental saddle–node.

The following results hold for any quadratic system:

(i) A straight line either has at most two (finite) contact points with a quadratic system (which include the singular points), or it is formed by trajectories of the system; see Lemma 11.1 of [Ye *et al.*, 1986]. We recall that by definition a *contact point* of a straight line L is a point of L where the vector field has the same direction as L, or it is zero.

(ii) If a straight line passing through two real finite singular points r_1 and r_2 of a quadratic system is not formed by trajectories, then it is divided by these two singular points in three segments $\overline{\infty r_1}$, $\overline{r_1 r_2}$ and $\overline{r_2 \infty}$ such that the trajectories cross $\overline{\infty r_1}$ and $\overline{r_2 \infty}$ in one direction, and they cross $\overline{r_1 r_2}$ in the opposite direction; see Lemma 11.4 of [Ye *et al.*, 1986].

(iii) If a quadratic system has a limit cycle, then it surrounds a unique singular point, and this point is a focus; see [Coppel, 1966].

(iv) A quadratic system with an invariant straight line has at most one limit cycle; see [Coll & Llibre, 1988].

(v) A quadratic system with more than one invariant straight line has no limit cycle; see [Bautin, 1954].

Proposition 4.1. *The border of any simply connected closed bidimensional set which is invariant under the flow of a vector field must either*

1) surround a singular point of index greater than or equal to +1, or

2) contain a singular point having an elliptic sector situated in the region delimited by the border, or

3) contain or surround an infinite number of singular points.

Proof. See the proof in [Artés *et al.*, 1998]. ■

5. Some algebraic and geometric concepts

In this article we use the concept of intersection number for curves (see [Fulton, 1969]). For a quick summary see Sec. 5 of [Artés *et al.*, 2006].

We shall also use the concepts of zero–cycle and divisor (see [Hartshorne, 1977])

as specified for quadratic vector fields in [Schlomiuk *et al.*, 2001]. For a quick summary see Sec. 6 of [Artés *et al.*, 2006]. See also [Llibre *et al.*, 2004].

We shall also use the concepts of invariant polynomials as used by the Sibirskii school for differential equations. For a quick summary see Sec. 7 of [Artés *et al.*, 2006].

In the next two sections we describe the algebraic invariants and T–comitants which are relevant in the study of families (7), see Sec. 6, and (8), see Sec. 7.

6. The bifurcation diagram of the systems in $\overline{QsnSN(A)}$

6.1. Bifurcation surfaces due to the changes in the nature of singularities

For systems (7) we will always have the origin as a finite singular point, a double saddle–node.

From Sec. 7 of [Artés *et al.*, 2008] we get the formulas which give the bifurcation surfaces of singularities in $\mathbb{R}^{12}$, produced by changes that may occur in the local nature of finite singularities. From [Schlomiuk *et al.*, 2005] we get equivalent formulas for the infinite singular points. These bifurcation surfaces are all algebraic and they are the following:

Bifurcation surfaces in $\mathbb{RP}^3$ due to multiplicities of singularities

$(\mathcal{S}_1)$ This is the bifurcation surface due to multiplicity of infinite singularities as detected by the coefficients of the divisor $D_{\mathbb{R}}(P, Q; Z) = \sum_{W \in \{Z=0\} \cap \mathbb{CP}^2} I_W(P, Q)W$, (here $I_W(P, Q)$ denotes the intersection multiplicity of $P = 0$ with $Q = 0$ at the point W situated on the line at infinity, i.e. $Z = 0$) whenever $deg((D_{\mathbb{R}}(P, Q; Z))) > 0$. This occurs when at least one finite singular point collides with at least one infinite point. More precisely this happens whenever the homogenous polynomials of degree two, p_2 and q_2, in p and q have a common root. In other words whenever $\mu = \mathrm{Res}_x(p_2, q_2)/y^4 = 0$. This is a quartic whose equation is

$$\mu = g^2(gk - 2hn + n^2) = 0.$$

$(\mathcal{S}_3)$[1] Since this family already has a saddle–node at the origin, the invariant $\mathbb{D}$, as defined in [Artés *et al.*, 2006], is always zero. The next T–comitant polynomial related to finite singularities is $\mathbb{T}$ as proved in [Artés *et al.*, 2008]. If this T–comitant polynomial vanishes, it may mean either the existence of another finite semi–elemental point, or the origin being a point of higher multiplicity, or the system being degenerate. The equation of this surface is

$$\mathbb{T} = g^4(h^2 - gk) = 0.$$

$(\mathcal{S}_5)$ Since this family already has a saddle–node at infinity, the invariant η, as defined in [Artés *et al.*, 2006], is always zero. In this sense, we have to consider a bifurcation related to the existence of either the double infinite singularity $\overline{\binom{0}{2}}SN$ plus a simple one, or a triple one. This phenomenon is ruled by the T–comitant $\widetilde{M}$ as proved in [Schlomiuk *et al.*, 2005, Artés *et al.*, 2012]. The equation of this surface is

$$\widetilde{M} = 2h - n = 0.$$

The surface of C^∞ bifurcation points due to a strong saddle or a strong focus changing the sign of their traces (weak saddle or weak focus)

$(\mathcal{S}_2)$ This is the bifurcation surface due to weak finite singularities, which occurs when the trace of a finite singular point is zero. The equation of this surface is given by

$$\mathcal{T}_4 = g^2(-4h^2 + 4gk + n^2) = 0,$$

where $\mathcal{T}_4$ is defined in [Vulpe, 2011]. This $\mathcal{T}_4$ is an invariant polynomial.

This bifurcation can produce a topological change if the weak point is a focus or just a C^∞ change if it is a saddle, except when this bifurcation coincides with a loop bifurcation associated with the same saddle, in which case, the change may also be topological.

The surface of C^∞ bifurcation due to a node becoming a focus

[1]The numbers attached to these bifurcations surfaces do not appear here in increasing order. We just kept the same enumeration used in [Artés *et al.*, 2006] to maintain coherence even though some of the numbers in that enumeration do not occur here.

($\mathcal{S}_6$) This surface will contain the points of the parameter space where a finite node of the system turns into a focus. This surface is a C^∞ but not a topological bifurcation surface. In fact, when we only cross the surface ($\mathcal{S}_6$) in the bifurcation diagram, the topological phase portraits do not change. However, this surface is relevant for isolating the regions where a limit cycle surrounding an antisaddle cannot exist. Using the results of [Artés *et al.*, 2008], the equation of this surface is given by $W_4 = 0$, where

$$\begin{aligned} W_4 =& g^4(-48h^4 + 32gh^2k + 16g^2k^2 + 64h^3n \\ & - 64ghkn - 24h^2n^2 + 24gkn^2 + n^4). \end{aligned}$$

Bifurcation surface in $\mathbb{RP}^3$ due to the presence of another invariant straight line apart from $\{y = 0\}$

($\mathcal{S}_4$) This surface will contain the points of the parameter space where another invariant straight line appears apart from $\{y = 0\}$. This surface is split in some regions. Depending on these regions, the straight line may contain connections of separatrices from different saddles or not. So, in some cases, it may imply a topological bifurcation and, in others, just a C^∞ bifurcation. The equation of this surface is given by

$$\text{Het} = h = 0.$$

These, except ($\mathcal{S}_4$), are all the bifurcation surfaces of singularities of systems (7) in the parameter space and they are all algebraic. We shall discover another bifurcation surface not necessarily algebraic and on which the systems have global connection of separatrices different from that given by ($\mathcal{S}_4$). The equation of this bifurcation surface can only be determined approximately by means of numerical tools. Using arguments of continuity in the phase portraits we can prove the existence of this not necessarily algebraic component in the region where it appears, and we can check it numerically. We shall name it the surface ($\mathcal{S}_7$).

We shall foliate the three–dimensional bifurcation diagram in $\mathbb{RP}^3$ by the planes $h = 0$ and $h = 1$, given by Proposition 2.4, plus the open half sphere $g = 0$ and we shall give pictures of the resulting bifurcation diagram on these planar sections on a disk or in an affine chart of $\mathbb{R}^2$.

The following two results study the geometrical behavior of the surfaces, that is, their singularities and their intersection points, or the points where two bifurcation surfaces are tangent.

In what follows we work in the chart of $\mathbb{RP}^3$ corresponding to $g \neq 0$, and we take $g = 1$. To do the study, we shall use Figs. 7 and 8 which are drawn on planes $h = h_0$ of $\mathbb{R}^3$, $h_0 \in \{0, 1\}$, having coordinates (h_0, k, n). In these planes the coordinates are (n, k) where the horizontal line is the n–axis.

As the final bifurcation diagram is quite complex, it is useful to introduce colors which will be used to talk about the bifurcation points:

(a) the curve obtained from the surface ($\mathcal{S}_1$) is drawn in blue (a finite singular point collides with an infinite one);

(b) the curve obtained from the surface ($\mathcal{S}_2$) is drawn in yellow (when the trace of a singular point becomes zero);

(c) the curve obtained from the surface ($\mathcal{S}_3$) is drawn in green (two finite singular points collide);

(d) the curve obtained from the surface ($\mathcal{S}_4$) is drawn in purple (presence of an invariant straight line). We draw it as a continuous curve if it implies a topological change or as a dashed curve if not.

(e) the curve obtained from the surface ($\mathcal{S}_5$) is drawn in red (three infinite singular points collide);

(f) the curve obtained from the surface ($\mathcal{S}_6$) is drawn in black (an antisaddle is on the edge of turning from a node to a focus or vice versa); and

(g) the curve obtained from the surface ($\mathcal{S}_7$) is also drawn in purple (same as for ($\mathcal{S}_4$)) since both surfaces deal with connections of separatrices mostly.

Lemma 6.1. *For $g \neq 0$ and $h = 0$, no surface, except ($\mathcal{S}_6$), has any singularity and all of the surfaces coincide at* $[1 : 0 : 0 : 0]$.

Proof. By setting $g = 1$ and restricting the equations of the surfaces to $h = 0$ we obtain: $\mu = k+n^2$, $\mathcal{T}_4 = 4k + n^2$, $\mathbb{T} = -k$, $\widetilde{M} = -n$, $W_4 = 16k^2 + 24kn^2 + n^4$ and Het $\equiv 0$. It is easy too see that μ, $\mathcal{T}_4$, $\mathbb{T}$, $\widetilde{M}$ and Het have no singularities as they are either a line, or a parabola, or null. Surface $(\mathcal{S}_6)$ is a quartic whose only singularity is at $[1 : 0 : 0 : 0]$ (this is the union of two parabolas having a common contact point). Besides, if we solve the system of equations formed by these expressions, we obtain $[1 : 0 : 0 : 0]$ as the unique solution. ■

Remark 6.2. Everywhere we mention "a contact point" we mean an intersection point between two curves with the same tangency of even order. Everywhere we mention "an intersection point" we mean a transversal intersection point (with different tangencies).

Lemma 6.3. *For $g \neq 0$ and $h = 1$, no surface, except $(\mathcal{S}_6)$, has any singularity. Moreover,*

1) *the point $[1 : 1 : 1 : 0]$ is a contact point among $(\mathcal{S}_2)$, $(\mathcal{S}_3)$ and $(\mathcal{S}_6)$;*

2) *the point $[1 : 1 : 1 : 1]$ is a contact point between $(\mathcal{S}_1)$ and $(\mathcal{S}_3)$;*

3) *the point $[1 : 1 : 1 : 2]$ is an intersection point between $(\mathcal{S}_3)$ and $(\mathcal{S}_5)$;*

4) *the point $[1 : 1 : 48/49 : 6/7]$ is an intersection point between $(\mathcal{S}_1)$ and $(\mathcal{S}_6)$;*

5) *the point $[1 : 1 : 8/9 : 2/3]$ is an intersection point between $(\mathcal{S}_2)$ and $(\mathcal{S}_6)$;*

6) *the point $[1 : 1 : 0 : -6]$ is an intersection point between $(\mathcal{S}_4)$ and $(\mathcal{S}_6)$;*

7) *the point $[1 : 1 : 0 : -2]$ is an intersection point between $(\mathcal{S}_2)$ and $(\mathcal{S}_4)$;*

8) *the point $[1 : 1 : 0 : 0]$ is an intersection point between $(\mathcal{S}_1)$ and $(\mathcal{S}_4)$;*

9) *the point $[1 : 1 : 0 : 2]$ is an intersection point among all the surfaces, except $(\mathcal{S}_3)$. Besides, surface $(\mathcal{S}_6)$ is singular at this point, surface $(\mathcal{S}_4)$ has a contact point with one of the components of $(\mathcal{S}_6)$ and $(\mathcal{S}_1)$ has a contact point with the other component of $(\mathcal{S}_6)$.*

Proof. Analogously to the previous lemma, by restricting the equations of the surfaces to $g = h = 1$ and solving the system of equation formed by pairs of the restricted expressions, we obtain the result. ■

Remark 6.4. Even though we are working in $\mathbb{RP}^3$, we have seen that the study can be reduced to the geometry of the curves obtained by intersecting the surfaces with this slice.

According to Proposition 2.4, we shall study the bifurcation diagram having as reference the values $h = 0$ and $h = 1$ (see Figs. 7 and 8) and also the value $h = \infty$, which corresponds to $g = 0$. We perform the bifurcation diagram of all singularities for $h = \infty$ $(g = 0)$ by putting $g = 0$ and in the remaining three variables (h, k, n), yielding the point $[h : k : n] \in \mathbb{RP}^2$, we take the chart $h \neq 0$ in which we may assume $h = 1$.

For these values of the parameters, system (7) becomes

$$\begin{aligned} \dot{x} &= 2xy + ky^2, \\ \dot{y} &= y + ny^2, \end{aligned} \tag{19}$$

and the expressions of the bifurcation surfaces for (19) are given by

$$\begin{gathered} \mu = \mathcal{T}_4 = \mathbb{T} = W_4 = \text{Het} = 0 \\ \text{and } \widetilde{M} = 2 - n. \end{gathered} \tag{20}$$

Remark 6.5. We note that $\{y = 0\}$ is a straight line formed by an infinite number of singularities for system (19). Then, the phase portraits of such a system must be studied by removing the common factor of the two equations defining it and studying the linear system that remains. The invariant polynomials for linear systems equivalent to the ones for quadratic systems that we use in this paper have not been defined, but they are trivial to use for a concrete normal form like (19).

The bifurcation curves of singularities (20) are shown in Fig. 6. We point out that, although we have drawn in blue the vertical axis k in Fig. 6, it does not represent surface $(\mathcal{S}_1)$ since it is null by equations (20), but it has the same geometrical meaning as this surface, i.e. a finite singular has gone to infinity.

We now describe the labels used for each part. The subsets of dimensions 3, 2, 1 and 0 of the parti-

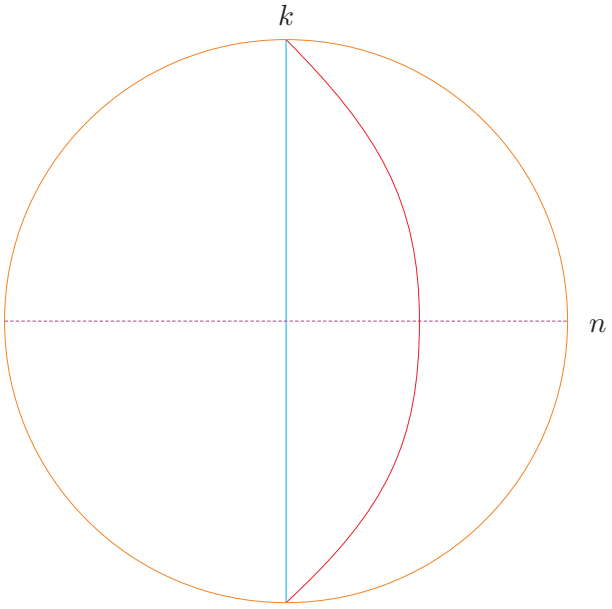

Fig. 6. Slice of the parameter space for (7) when $h = \infty$.

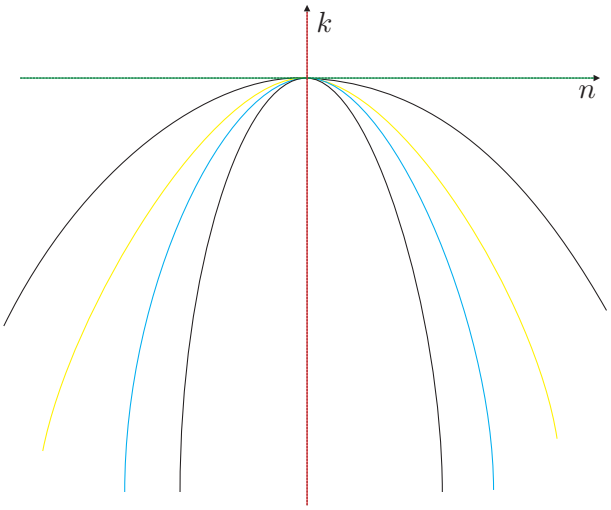

Fig. 7. Slice of the parameter space for (7) when $h = 0$.

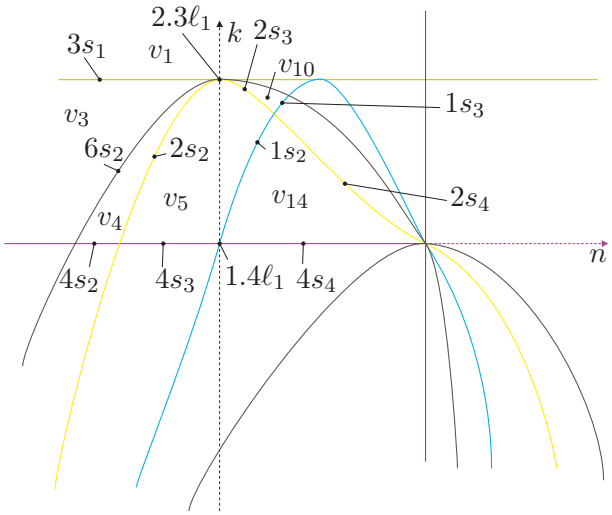

Fig. 8. Slice of the parameter space for (7) when $h = 1$.

tion of the parameter space will be denoted respectively by V, S, L and P for Volume, Surface, Line and Point, respectively. The surfaces are named using a number which corresponds to each bifurcation surface which is placed on the left side of the letter S. To describe the portion of the surface we place an index. The curves that are intersection of surfaces are named by using their corresponding numbers on the left side of the letter L, separated by a point. To describe the segment of the curve we place an index. Volumes and Points are simply indexed (since three or more surfaces may be involved in such an intersection). Furthermore, we also add a super–index which will be different for every topologically distinct phase portrait. We shall use this super–index when related to phase portraits, but we may skip it while studying the bifurcation diagram.

We consider an example: the surface $(\mathcal{S}_1)$ splits into 6 different two–dimensional parts labeled from $1S_1$ to $1S_6$, plus some one–dimensional arcs labeled as $1.iL_j$ (where i denotes the other surface intersected by $(\mathcal{S}_1)$ and j is a number), and some zero–dimensional parts. In order to simplify the labels in Figs. 11 to 13 we see **V1** which stands for the TEX notation V_1. Analogously, **1S1** (respectively, **1.2L1**) stands for $1S_1$ (respectively, $1.2L_1$). And the same happens with other pictures.

Remark 6.6. We point out that the slice $h = \infty$ is a bifurcation surface in the parameter space and receives the label $9S$. We have denoted the curved

segments in which the equator splits as $8.9L_j$.

As an exact drawing of the curves produced by intersecting the surfaces with slices gives us very small regions which are difficult to distinguish, and points of tangency are almost impossible to recognize, we have produced topologically equivalent pictures where regions are enlarged and tangencies are easy to observe. The reader may find the exact pictures in the web page http://mat.uab.es/∼artes/articles/qvfsn2SN02/qvfsn2SN02.html.

Remark 6.7. We consider $g \neq 0$. It is worth mentioning that if we compare the case of the slices $h = 0$ and $h = 1$ (here we may take any other $h > 0$), we see that a region looking like a "cross" appears on the slice $h = 1$ between $(\mathcal{S}_3)$ $(n = 1)$ and $(\mathcal{S}_4)$ $(n = 0)$ and also between $(\mathcal{S}_5)$ $(k = 2)$ and $k = 0$. This "cross" exists on every slice given by $h > 0$ and, as we take $h \to 0$, the region inside the "cross" including the borders tends to the two axes. Furthermore, the rectangle in the middle of the cross tends to $[1 : 0 : 0 : 0]$.

We recall that the black surface $(\mathcal{S}_6)$ (or W_4) means the turning of a finite antisaddle from a node to a focus. Then, according to the general results about quadratic systems, we could have limit cycles around such point.

Remark 6.8. Wherever two parts of equal dimension d are separated only by a part of dimension $d - 1$ of the black bifurcation surface $(\mathcal{S}_6)$, their respective phase portraits are topologically equivalent since the only difference between them is that a finite antisaddle has turned into a focus without change of stability and without appearance of limit cycles. We denote such parts with different labels, but we do not give specific phase portraits in pictures attached to Theorems 1.1 and 1.2 for the parts with the focus. We only give portraits for the parts with nodes, except in the case of existence of a limit cycle or a graphic where the singular point inside them is portrayed as a focus. Neither do we give specific invariant description in Sec. 9 distinguishing between these nodes and foci.

6.2. Bifurcation surfaces due to connections

We now describe for each set of the partition on $g \neq 0$ and $h = 1$ the local behavior of the flow around all the singular points. Given a concrete value of parameters of each one of the sets in this slice we compute the global phase portrait with the numerical program P4 [Dumortier *et al.*, 2006]. It is worth mentioning that many (but not all) of the phase portraits in this paper can be obtained not only numerically but also by means of perturbations of the systems of codimension one higher.

In this slice we have a partition in 2–dimensional regions bordered by curved polygons, some of them bounded, others bordered by infinity. Provisionally, we use low–case letters to describe the sets found algebraically so as not to interfere with the final partition described with capital letters. For each 2–dimensional region we obtain a phase portrait which is coherent with those of all their borders, except in one region. Consider the set v_1 in Fig. 8. In it we have only a saddle–node as finite singularity. When reaching the set $2.3\ell_1$, we are on surfaces $(\mathcal{S}_2)$, $(\mathcal{S}_3)$ and $(\mathcal{S}_6)$ at the same time; this implies the presence of one more finite singularity (in fact, it is a cusp point) which is on the edge of splitting itself and give birth to finite saddle and antisaddle. Now, we consider the segments $2s_2$ and $2s_3$. By the Main Theorem of [Vulpe, 2011], the corresponding phase portraits of these sets have a first–order weak saddle and a first–order weak focus, respectively. So, on $2s_3$ we have a Hopf bifurcation. This means that either in v_5 or v_{10} we must have a limit cycle. In fact this occurs in v_5. Indeed, as we have a weak saddle on $2s_2$ and we have not detected a loop-type bifurcation surface intersecting this subset, neither its presence is forced to keep the coherence, its corresponding phase portrait is topologically equivalent to the portraits of v_4 and v_5. Since in v_5 we have a phase portrait topologically equivalent to the one on $2s_2$ (without limit cycles) and a phase portrait with limit cycles, this region must be split into two other ones separated by a new surface $(\mathcal{S}_7)$ having at least one element $7S_1$ such that one region has limit cycle and the other does not, and the border $7S_1$ must correspond to a connection between separatrices. After numerical computations we checked that the region v_5 splits into V_5 without limit cycles

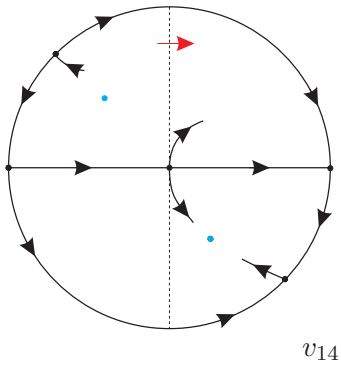

Fig. 9. The local behavior around each of the finite and infinite singularities of any representant of v_{14}. The red arrow shows the sense of the flow along the y-axis and the blue points are the focus and the node with same stability.

and V_{11} with one limit cycle, both of which can be seen in Fig. 13.

The next result assures us the existence of limit cycle in any representative of the subset v_{14} and it is needed to complete the study of $7S_1$.

Lemma 6.9. *In v_{14} there is always one limit cycle.*

Proof. We see that the subset v_{14} is characterized by $\mu < 0$, $\mathcal{T}_4 < 0$, $W_4 < 0$, $\widetilde{M} > 0$, $\mathbb{T} > 0$, $k > 0$ and $n > 0$. Any representative of v_{14} has the finite saddle–node at the origin with its eigenvectors on the axes and two more finite singularities, a focus and a node (the focus is due to $W_4 < 0$). We claim that these two other singularities are placed in symmetrical quadrants with respect to the origin (see Fig. 9). In fact, by computing the exact expression of each singular point (x_1, y_1) and (x_2, y_2) and multiplying their x–coordinates and y-coordinates we obtain k/μ and $1/\mu$, respectively, which are always negative since $k > 0$ and $\mu < 0$ in v_{14}. Besides, each one of them is placed in an even quadrant since the product of the coordinates of each antisaddles is never null and any representative gives a negative product. Moreover, both antisaddles have the same stability since the product of their traces is given by $\mu/\mathcal{T}_4$ which is always positive in v_{14}.

The infinite singularities of systems in v_{14} are the saddle–node $\binom{0}{2}SN$ (recall the normal form (7)) and a saddle. In fact, the expression of the singular points in the local chart U_1 are $(0, 0)$ and $((-2h + n)/k, 0)$. We note that the determinant of the Jacobian matrix of the flow in U_1 at the second singularity is given by

$$-\frac{(2h-n)^2\left(2hn-k-n^2\right)}{k^2} = \frac{\widetilde{M}^2\mu}{k^2},$$

which is negative since $\mu < 0$ in v_{14}. Besides, this pair of saddles are in the second and the fourth quadrant because its first coordinate $(-2h+n)/k = -\widetilde{M}/k$ is negative since $\widetilde{M} > 0$ and $k > 0$ in v_{14}.

We also note that the flow along the y-axis is such that $\dot{x} > 0$.

Since we have a pair of saddle points in the even quadrants, each one of the finite antisaddles is in an even quadrant, no orbit can enter into the second quadrant and no orbit may leave the fourth one and, in addition, these antisaddles, a focus and a node, have the same stability, any phase portrait in v_{14} must have at least one limit cycle in any of the even quadrants. Moreover, the limit cycle is in the second quadrant, because the focus is there since a saddle–node is born in that quadrant at $3s_1$, splits in two points when entering v_3 (both remain in the same quadrant since $x_1x_2 = k/\mu < 0$ and $y_1y_2 = 1/\mu < 0$), the node turns into focus at $6s_2$ and the saddle moves to infinity on $1s_2$ appearing as a node at the fourth quadrant when entering v_{14}. Furthermore, by the statement (iv) of Sec. 4, it follows the uniqueness of the limit cycle in v_{14}. ■

Now, the following result states that the segment which splits the subset v_5 into the regions V_5 and V_{11} has its endpoints well–determined. We can visualize the image of this surface in the plane $h = 1$ in Fig. 13.

Proposition 6.10. *The endpoints of the part of the curve $7S_1$ are $2.3\ell_1$, intersection of surfaces $(\mathcal{S}_2)$ and $(\mathcal{S}_3)$, and $1.4\ell_1$, intersection of surfaces $(\mathcal{S}_1)$ and $(\mathcal{S}_4)$.*

Proof. We write $r_1 = [1 : 1 : 0 : 2]$ and $r_2 = [1 : 1 : 1 : 0]$ for $2.3\ell_1$ and $1.4\ell_1$, respectively. If the starting point were any point of the segments $2s_2$ or $2s_3$, we would have the following incoherences: firstly, if the starting point of $7S_1$ were on $2s_2$, a portion of this subset must refer to a Hopf bifurcation since we have a limit cycle in V_{11}; and secondly, if this starting point were on $2s_3$, a portion of this subset must not refer to a Hopf bifurcation which

contradicts the fact that on $2s_3$ we have a first–order weak focus. Finally, the ending point must be r_2 because, if it were located on $4s_3$, we would have a segment between this point and $1.4\ell_1$ along surface $(\mathcal{S}_4)$ with two invariant straight lines and one limit cycle, which contradicts the statement (v) of Sec. 4, and if it were on $1s_2$, we would have a segment between this point and $1.4\ell_1$ along surface $(\mathcal{S}_1)$ without limit cycle which is not compatible with Lemma 6.9 since $\mu = 0$ does not produce a graphic. ■

In Fig. 10 we show the sequence of phase portraits along the subsets pointed out in Fig. 8.

We cannot be totally sure that this is the unique additional bifurcation curve in this slice. There could exist others which are closed curves which are small enough to escape our numerical research, but the one located is enough to maintain the coherence of the bifurcation diagram. We recall that this kind of studies are always done modulo "islands". For all other two–dimensional parts of the partition of this slice whenever we join two points which are close to two different borders of the part, the two phase portraits are topologically equivalent. So we do not encounter more situations than the one mentioned above.

In Figs. 11 to 13 we show the bifurcation diagrams for family (7). Since there are two relevant values of h to be taken into consideration (according to Proposition 2.4) plus the infinity, the pictures show all the algebraic bifurcation curves and all the non-algebraic bifurcation ones needed for the coherence of the diagram, which lead to a complete bifurcation diagram for family (7) modulo islands. In Sec. 9 the reader can look for the topological equivalences among the phase portraits appearing in the various parts and the selected notation for their representatives in Figs. 1 and 2. In Fig. 13, we have colored in light yellow the regions with one limit cycle.

7. The bifurcation diagram of the systems in $\overline{QsnSN(B)}$

Before we describe all the bifurcation surfaces for $\overline{QsnSN(B)}$, we prove the following result which gives conditions on the parameters for the presence of either a finite star node n^* (whenever any two distinct non–trivial integral curves arrive at the node with distinct slopes), or a finite dicritical node n^d (a node with identical eigenvalues but Jacobian non–diagonal).

Lemma 7.1. *Systems* (8) *always have a* n^**, if* $m = 0$ *and* $h \neq 0$*, or a* n^d*, otherwise.*

Proof. We note that the singular point $(0, -1/2h)$ has its Jacobian matrix given by

$$\begin{pmatrix} -1 & 0 \\ -m/h & -1 \end{pmatrix}.$$

■

7.1. Bifurcation surfaces due to the changes in the nature of singularities

The needed invariant and T–comitant polynomials needed here are the same as in the previous system except surfaces $(\mathcal{S}_4)$ and $(\mathcal{S}_6)$; so we shall only give the geometrical meaning and their equations plus a deeper discussion on surface $(\mathcal{S}_6)$. For further information about them, see Sec. 6.

Bifurcation surfaces in $\mathbb{RP}^3$ due to multiplicities of singularities

$(\mathcal{S}_1)$ This is the bifurcation surface due to the multiplicity of infinite singularities. This occurs when at least one finite singular point collides with at least one infinite point. The equation of this surface is

$$\mu = 4h^2(g^2 + 2h\ell - 2gm) = 0.$$

$(\mathcal{S}_3)$ This is the bifurcation surface is due to either the existence of another finite semi–elemental point, or the origin being a higher multiplicity point, or the system being degenerate. The equation of this surface is given by

$$\mathbb{T} = -g^2h^2 = 0.$$

It only has substantial importance when we consider the planes $g = 0$ or $h = 0$.

$(\mathcal{S}_5)$ This is the bifurcation surface due to the collision of infinite singularities, i.e. when all three infinite singular points collide. The equation of this surface is

$$\widetilde{M} = (g - 2m)^2 = 0.$$

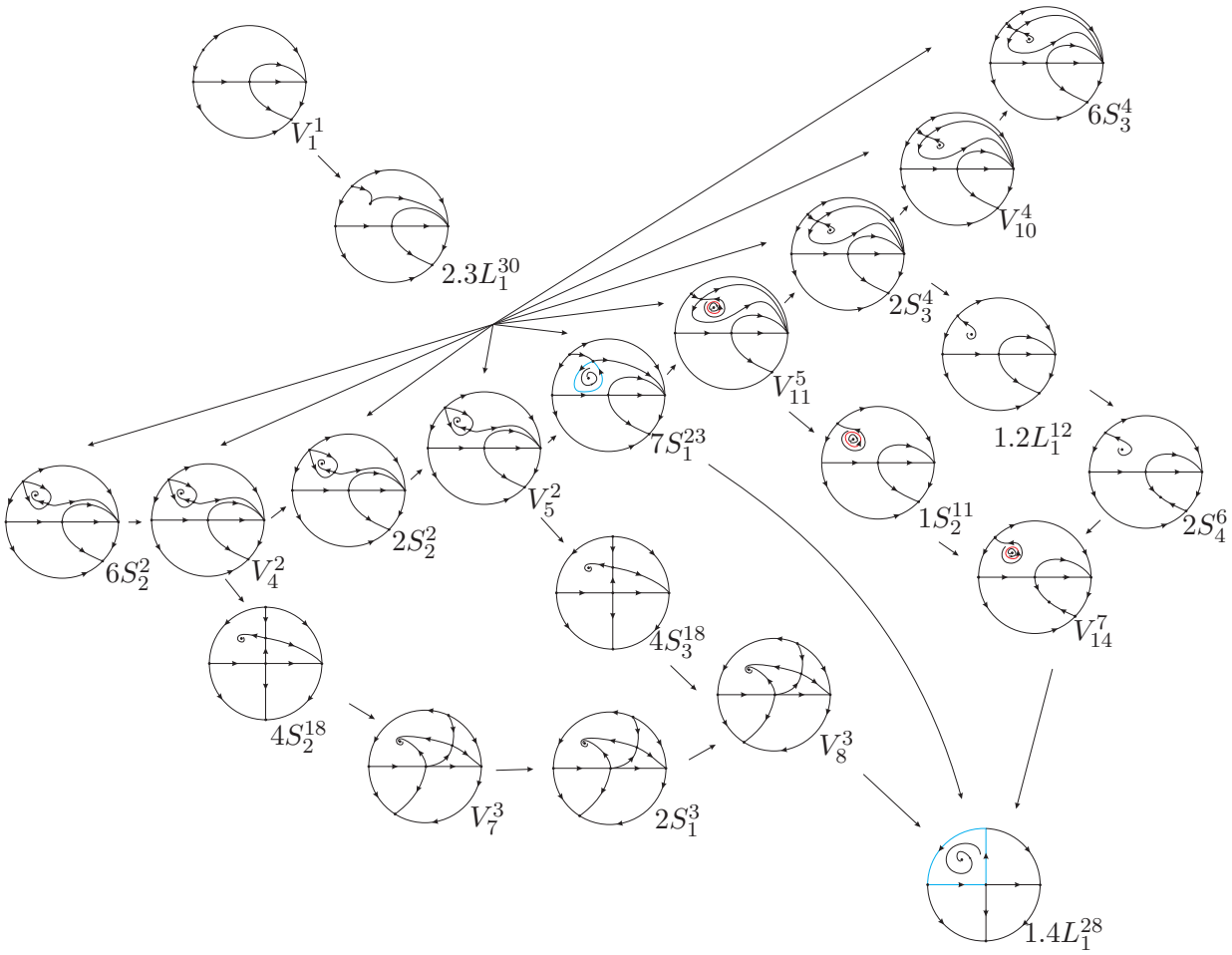

Fig. 10. Sequence of phase portraits in slice $g = h = 1$ from v_1 to $1.8\ell_1$. We start from v_1. When crossing $2.3\ell_1$, we may choose at least seven "destinations": $6s_2$, v_4, $2s_2$, v_5, $2s_3$, v_{10} and $6s_3$. In each one of these subsets, but v_5, we obtain only one phase portrait. In v_5 we find (at least) three different ones, which means that this subset must be split into (at least) three different regions whose phase portraits are V_5^2, $7S_1^{23}$ and V_{11}^5. And then we shall follow the arrows to reach the subset $1.4\ell_1$ whose corresponding phase portrait is $1.4L_1^{28}$.

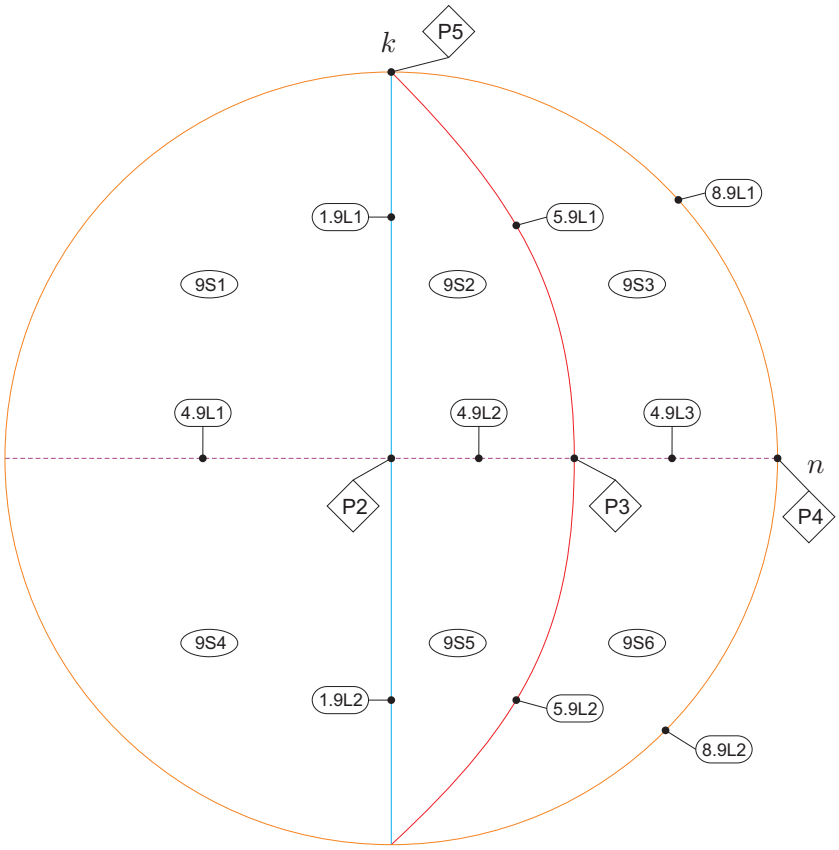

Fig. 11. Complete bifurcation diagram of $\overline{QsnSN(A)}$ for slice $h = \infty$.

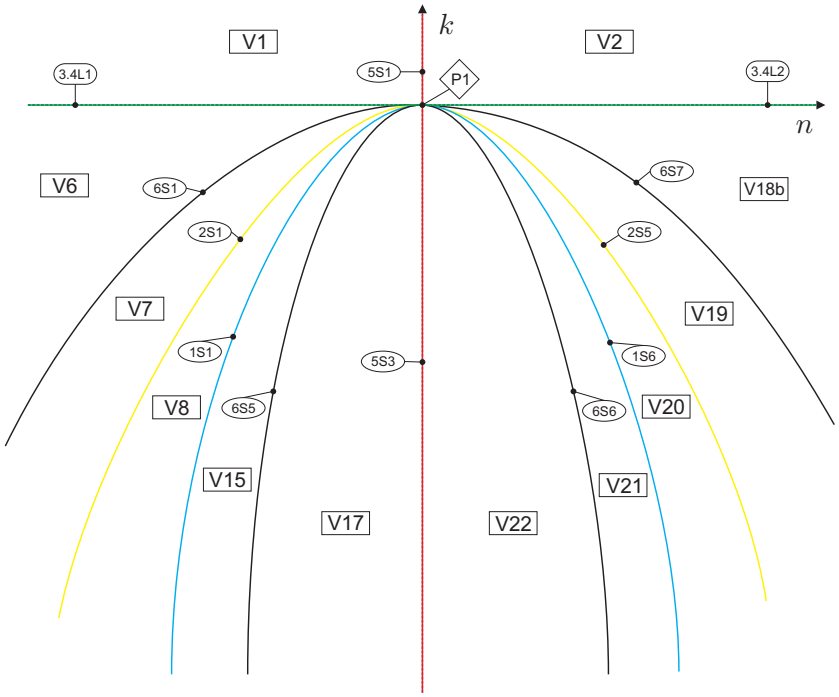

Fig. 12. Complete bifurcation diagram of $\overline{QsnSN(A)}$ for slice $h = 0$.

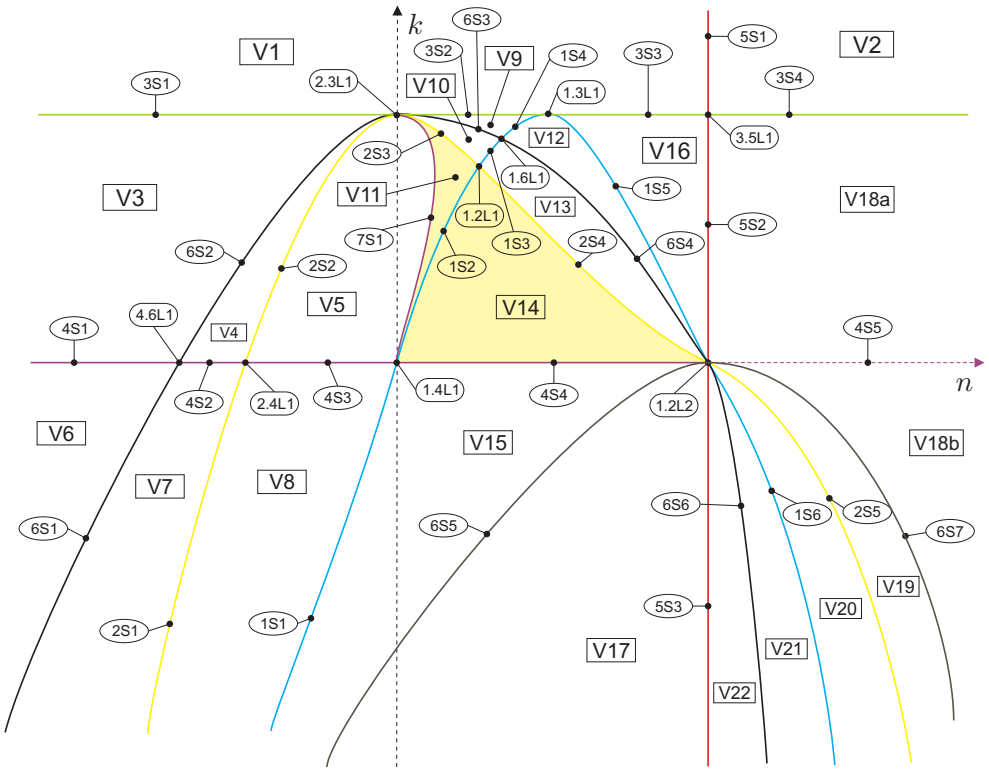

Fig. 13. Complete bifurcation diagram of $\overline{QsnSN(A)}$ for slice $h = 1$.

The surface of C^∞ bifurcation due to a strong saddle or a strong focus changing the sign of their traces (weak saddle or weak focus)

$(\mathcal{S}_2)$ This is the bifurcation surface due to weak finite singularities, which occurs when their trace is zero. The equation of this surface is given by

$$\mathcal{T}_4 = -16h^3\ell = 0.$$

The surface of C^∞ bifurcation due to a node becoming a focus

$(\mathcal{S}_6)$ Since W_4 is identically zero for all the bifurcation space, the invariant that captures if a second point may be on the edge of changing from node to focus is W_3. The equation of this surface is given by

$$W_3 = 64h^4(g^4 + 2g^2h\ell + h^2\ell^2 - 2g^3m) = 0.$$

These are all the bifurcation surfaces of singularities of the systems (8) in the parameter space and they are all algebraic. We do not expect to discover any other bifurcation surface (neither non-algebraic nor algebraic one) due to the fact that in all the transitions we make among the parts of the bifurcation diagram of this family we find coherence in the phase portraits when "traveling" from one part to the other.

Analogously to the previous class, we shall foliate the three–dimensional bifurcation diagram in $\mathbb{RP}^3$ by the planes $h = 0$ and $h = 1$, given by Proposition 2.7, plus the open half sphere $g = 0$ and we shall give pictures of the resulting bifurcation diagram on these planar sections on a disk or in an affine chart of $\mathbb{R}^2$.

The following three results study the geometrical behavior of the surfaces, that is, their singularities and the simultaneous intersection points among them, or the points where two bifurcation surfaces are tangent, and the presence of a different invariant straight line in the particular case when $\ell = 0$.

In what follows we work in the chart of $\mathbb{RP}^3$ corresponding to $g \neq 0$, and we take $g = 1$. To do the study, we shall use Figs. 15 and 16 which are drawn on planes $h = h_0$ of $\mathbb{R}^3$, $h_0 \in \{0, 1\}$, having coordinates (h_0, ℓ, m). In these planes the coordinates are (ℓ, m) where the horizontal line is the ℓ–axis.

We shall use the same set of colors for the bifurcation surfaces as in the previous case.

Lemma 7.2. *All the bifurcation surfaces intersect on $h = 0$, with $g \neq 0$.*

Proof. The equations of surfaces $(\mathcal{S}_1)$, $(\mathcal{S}_2)$, $(\mathcal{S}_3)$ and $(\mathcal{S}_6)$ are identically zero when restricted to the plane $h = 0$, and the equation of $(\mathcal{S}_5)$ is the straight line $2m - 1 = 0$, for all $g \neq 0$, $h \geq 0$ and $m, \ell \in \mathbb{R}$. ■

Lemma 7.3. *For $h = 1$ (with $g \neq 0$), the surfaces have no singularities. Moreover,*

1) *the point $[1 : 1 : -2 : 1/2]$ is an intersection point between $(\mathcal{S}_5)$ and $(\mathcal{S}_6)$;*

2) *the point $[1 : 1 : 0 : 1/2]$ is an intersection point among $(\mathcal{S}_1)$, $(\mathcal{S}_2)$, $(\mathcal{S}_5)$ and $(\mathcal{S}_6)$. Besides, the intersection between $(\mathcal{S}_1)$ and $(\mathcal{S}_6)$ is in fact a contact point.*

Proof. For $g = h = 1$, surface $(\mathcal{S}_1)$ is the straight line $1 + 2\ell - 2m = 0$, which intersects surface $(\mathcal{S}_5)$, which is a double straight line with equation $-1 + 2m = 0$, at the point $[1 : 1 : 0 : 1/2]$; surface $(\mathcal{S}_6)$ is the parabola $1 + 2\ell + \ell^2 - 2m = 0$ passing through the point $[1 : 1 : 0 : 1/2]$ with a 2–order contact with surface $(\mathcal{S}_1)$; moreover, surface $(\mathcal{S}_6)$ has another intersection point with surface $(\mathcal{S}_5)$ at $[1 : 1 : -2 : 1/2]$; surface $(\mathcal{S}_2)$ is the straight line $\ell = 0$, which intersects surfaces $(\mathcal{S}_1)$, $(\mathcal{S}_5)$ and $(\mathcal{S}_6)$ at the point $[1 : 1 : 0 : 1/2]$. ■

Lemma 7.4. *If $\ell = 0$, the straight line $\{y = 0\}$ is invariant under the flow of* (8).

Proof. It is easy to check the result by substituting $\ell = 0$ in (8). ■

According to Proposition 2.7, we shall study the bifurcation diagram having as reference the values $h = 0$ and $h = 1$ (see Figs. 15 and 16) and also the value $h = \infty$, which corresponds to $g = 0$. We perform the bifurcation diagram of all singularities for $h = \infty$ $(g = 0)$ by putting $g = 0$ and in the remaining three variables (h, ℓ, m), yielding the point $[h : \ell : m] \in \mathbb{RP}^2$, we take the chart $h \neq 0$ in which we may assume $h = 1$.

For these values of the parameters, system (8) becomes

$$\begin{aligned} \dot{x} &= 2xy, \\ \dot{y} &= y + \ell x^2 + 2mxy, \end{aligned} \tag{21}$$

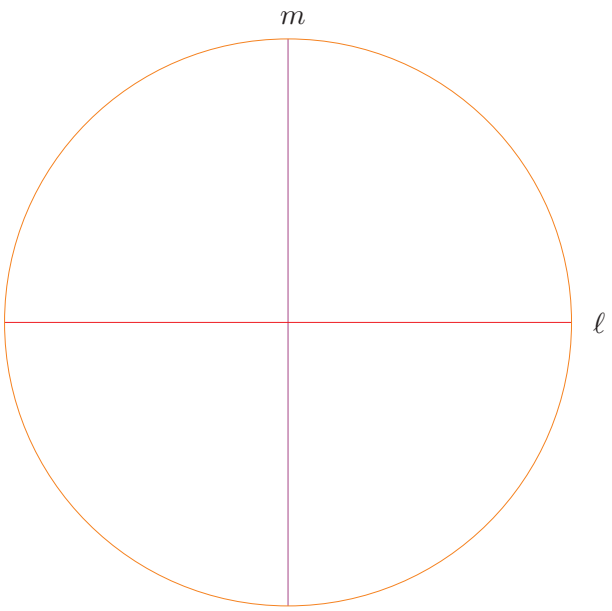

Fig. 14. Slice of parameter space for (8) when $h = \infty$.

and the expressions of the bifurcation surfaces for (21) are given by

$$\begin{array}{c} \mu = 8\ell,\ \mathcal{T}_4 = -16\ell,\ \mathbb{T} = 0, \\ \widetilde{M} = 4m^2 \text{ and } W_3 = 64\ell^2. \end{array} \tag{22}$$

Remark 7.5. We note that $\{y = 0\}$ is a straight line of singularities for system (21) when $\ell = 0$. To study the phase portraits of system (21), we proceed as stated in Remark 6.5.

The bifurcation curves of singularities (22) are shown in Fig. 14.

Here we also give topologically equivalent figures to the exact drawings of the bifurcation curves. The reader may find the exact pictures in the web page http://mat.uab.es/∼artes/articles/qvfsn2SN02/qvfsn2SN02.html.

We recall that the black surface ($\mathcal{S}_6$) (or W_3) means the turning of a finite antisaddle from a node to a focus. Then, according to the general results about quadratic systems, we could have limit cycles around such focus for any set of parameters having $W_3 < 0$.

In Figs. 17 to 19 we show the bifurcation diagrams for family (8). Since there are two relevant values of h to be taken into consideration (according to Proposition 2.7) plus the infinity, the pictures

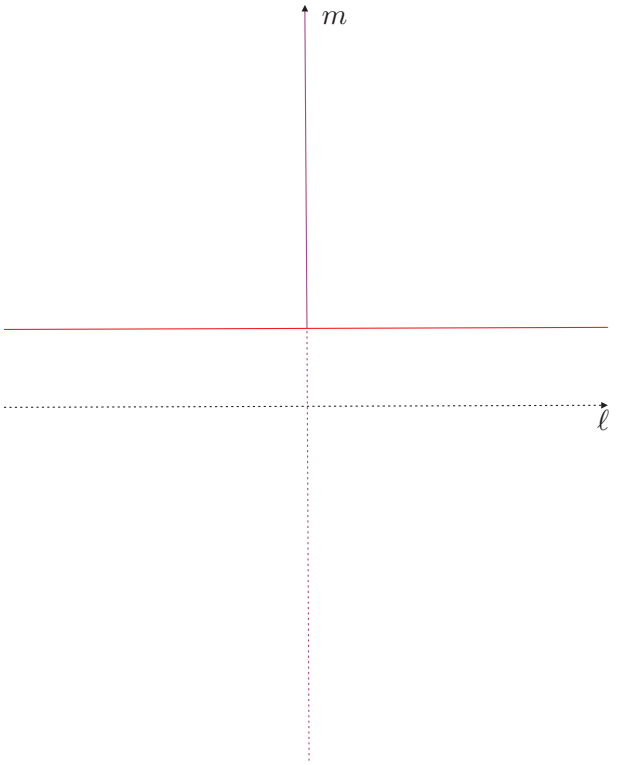

Fig. 15. Slice of parameter space for (8) when $h = 0$.

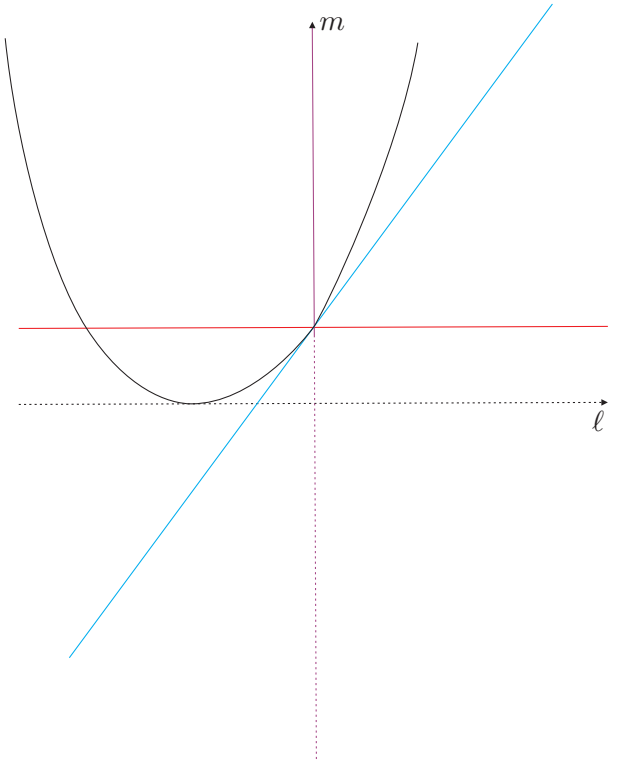

Fig. 16. Slice of parameter space for (8) when $h = 1$.

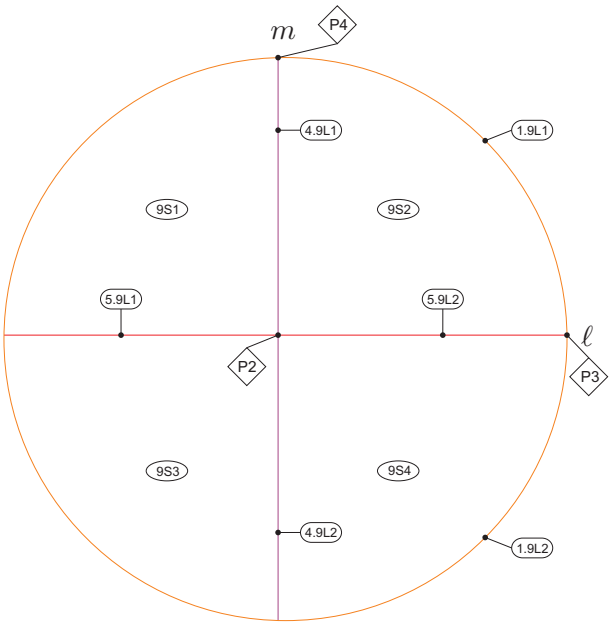

Fig. 17. Complete bifurcation diagram of $\overline{QsnSN(B)}$ for slice $h = \infty$.

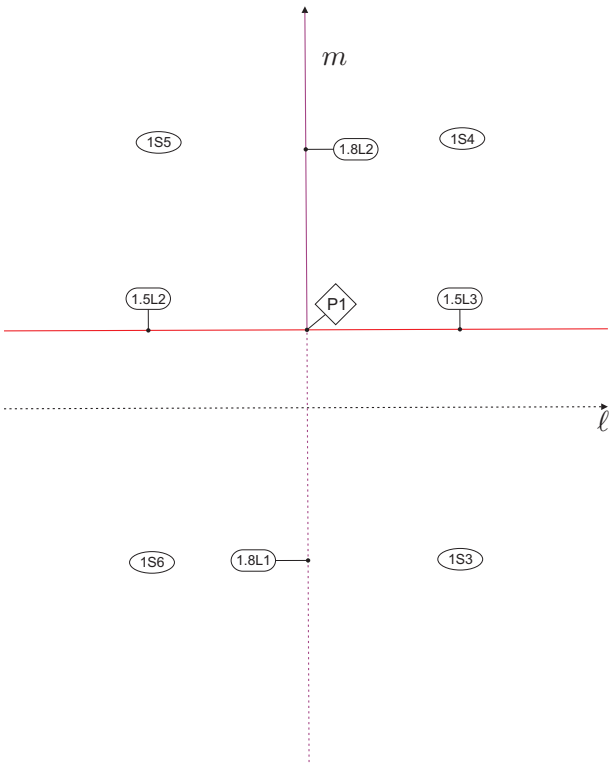

Fig. 18. Complete bifurcation diagram of $\overline{QsnSN(B)}$ for slice $h = 0$.

show all the algebraic bifurcation curves obtained by the invariant polynomials. We observe that non-algebraic bifurcation curves were not needed for the coherence of the diagram. All of these leads to a complete bifurcation diagram for family (8) modulo islands. In Sec. 9 the reader can look for the topological equivalences among the phase portraits appearing in the various parts and the selected notation for their representatives in Fig. 3.

8. Other relevant facts about the bifurcation diagrams

The bifurcation diagrams we have obtained for the families $\overline{QsnSN(A)}$ and $\overline{QsnSN(B)}$ are completely coherent, i.e. in each family, by taking any two points in the parameter space and joining them by a continuous curve, along this curve the changes in phase portraits that occur when crossing the different bifurcation surfaces we mention can be completely explained.

Nevertheless, we cannot be sure that these bifurcation diagrams are the complete bifurcation diagrams for $\overline{QsnSN(A)}$ and $\overline{QsnSN(B)}$ due to the possibility of "islands" inside the parts bordered by unmentioned bifurcation surfaces. In case they exist, these "islands" would not mean any modifica-

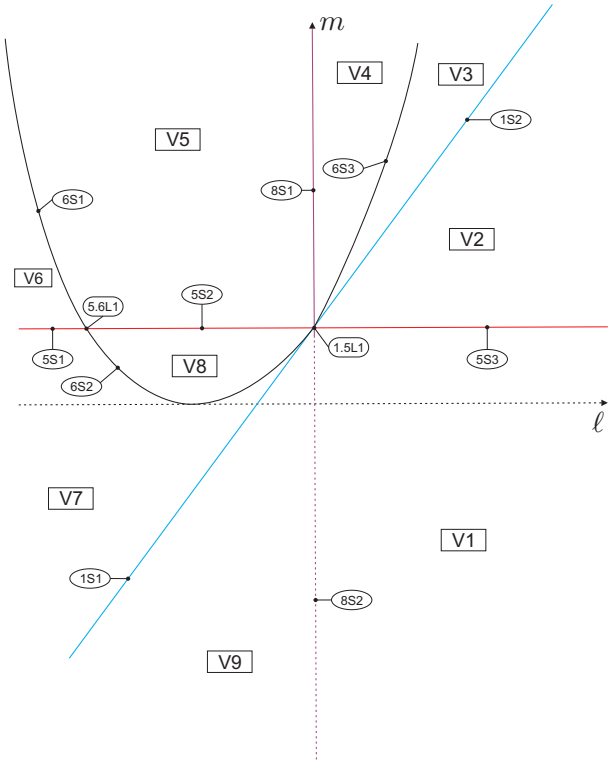

Fig. 19. Complete bifurcation diagram of $\overline{QsnSN(B)}$ for slice $h = 1$.

tion of the nature of the singular points. So, on the border of these "islands" we could only have bifurcations due to saddle connections or multiple limit cycles.

In case there were more bifurcation surfaces, we should still be able to join two representatives of any two parts of the 85 parts of $\overline{QsnSN(A)}$ or the 43 parts of $\overline{QsnSN(B)}$ found until now with a continuous curve either without crossing such bifurcation surface or, in case the curve crosses it, it must do it an even number of times without tangencies, otherwise one must take into account the multiplicity of the tangency, so the total number must be even. This is why we call these potential bifurcation surfaces "*islands*".

However, in none of the two families we have found a different phase portrait which could fit in such an island. The existence of the invariant straight line avoids the existence of a double limit cycle which is the natural candidate for an island (recall the item (iv) of Sec. 4), and also the limited number of separatrices (compared to a generic case) limits greatly the possibilities for phase portraits.

9. Completion of the proofs of Theorems 1.1 and 1.2

In the bifurcation diagram we may have topologically equivalent phase portraits belonging to distinct parts of the parameter space. As here we have finitely many distinct parts of the parameter space, to help us identify or to distinguish phase portraits, we need to introduce some invariants and we actually choose integer–valued invariants. All of them were already used in [Llibre *et al.*, 2004, Artés *et al.*, 2006]. These integer–valued invariants, and sometimes symbol–valued invariants, yield a classification which is easier to grasp.

Definition 9.1. We denote by $I_1(S)$ the number of the isolated real finite singular points. This invariant is also denoted by $\mathbb{N}_{\mathbb{R},f}(S)$ [Artés *et al.*, 2006].

Definition 9.2. We denote by $I_2(S)$ the sum of the indices of the real finite singular points. This invariant is also denoted by $\deg(DI_f(S))$ [Artés *et al.*, 2006].

Definition 9.3. We denote by $I_3(S)$ the number of the real infinite singular points. This number can be ∞ in some cases. This invariant is also denoted by $\mathbb{N}_{\mathbb{R},\infty}(S)$ [Artés *et al.*, 2006].

Definition 9.4. We denote by $I_4(S)$ the sequence of digits (each one ranging from 0 to 4) such that each digit describes the total number of global or local separatrices (different from the line of infinity) ending (or starting) at an infinite singular point. The number of digits in the sequences is 2 or 4 according to the number of infinite singular points. We can start the sequence at anyone of the infinite singular points but all sequences must be listed in a same specific order either clockwise or counter–clockwise along the line of infinity.

In our case we have used the clockwise sense beginning from the saddle–node at the origin of the local chart U_1 in the pictures shown in Figs. 1 and 2, and the origin of the local chart U_2 in the pictures shown in Fig. 3.

Definition 9.5. We denote by $I_5(S)$ a digit which gives the number of limit cycles.

As we have noted previously in Remark 6.8, we do not distinguish between phase portraits whose only difference is that in one we have a finite node and in the other a focus. Both phase portraits are topologically equivalent and they can only be distinguished within the C^1 class. In case we may want to distinguish between them, a new invariant may easily be introduced.

Definition 9.6. We denote by $I_6(S)$ the digit 0 or 1 to distinguish the phase portrait which has connection of separatrices outside the straight line $\{y = 0\}$; we use the digit 0 for not having it and 1 for having it.

Definition 9.7. We denote by $I_7(S)$ the sequence of digits (each one ranging from 0 to 3) such that each digit describes the total number of global or local separatrices ending (or starting) at a finite antisaddle.

The next three invariants are needed to classify the degenerate phase portraits.

Definition 9.8. We denote by $I_8(S)$ the index of

the isolated infinite singular point when there exists another infinite singular which is located in the extreme of a curve of singularities.

Definition 9.9. We denote by $I_9(S)$ a digit which gives the number of lines with an infinite number of singularities.

Definition 9.10. We denote by $I_{10}(S)$ a symbol to represent the configuration of the curves of singularities. The symbols are: "><" to represent a hyperbola, "∪" to represent a parabola and "×" to represent two crossing lines.

Theorem 9.11. *Consider the subfamily* $\overline{QsnSN(A)}$ *which is the closure of all quadratic systems with a finite saddle–node* $\overline{sn}_{(2)}$ *and an infinite saddle–node of type* $\binom{\overline{0}}{2}$ *SN located in the direction defined by the eigenvector with null eigenvalue. Consider now all the phase portraits that we have obtained for this family. The values of the affine invariant* $\mathcal{I} = (I_1, I_2, I_3, I_4, I_5, I_6, I_8, I_9)$ *given in the following diagram yield a partition of these phase portraits of the family* $\overline{QsnSN(A)}$.

Furthermore, for each value of $\mathcal{I}$ *in this diagram there corresponds a single phase portrait; i.e.* S *and* S' *are such that* $I(S) = I(S')$, *if and only if* S *and* S' *are topologically equivalent.*

Theorem 9.12. *Consider the subfamily* $\overline{QsnSN(B)}$ *which is the closure of all quadratic systems with a finite saddle–node* $\overline{sn}_{(2)}$ *and an infinite saddle–node of type* $\binom{\overline{0}}{2}$ *SN located in the direction defined by the eigenvector with non–null eigenvalue. Consider now all the phase portraits that we have obtained for this family. The values of the affine invariant* $\mathcal{I} = (I_1, I_2, I_3, I_4, I_7, I_8, I_{10})$ *given in the following diagram yield a partition of these phase portraits of the family* $\overline{QsnSN(B)}$.

Furthermore, for each value of $\mathcal{I}$ *in this diagram there corresponds a single phase portrait; i.e.* S *and* S' *are such that* $I(S) = I(S')$, *if and only if* S *and* S' *are topologically equivalent.*

The bifurcation diagram for $\overline{QsnSN(A)}$ has 85 parts which produce 38 topologically different phase portraits as described in Tables 1 and 2. The remaining 47 parts do not produce any new phase portrait which was not included in the 38 previous ones. The difference is basically the presence of a strong focus instead of a node and vice versa.

Similarly, the bifurcation diagram for $\overline{QsnSN(B)}$ has 43 parts which produce 25 topologically different phase portraits as described in Tables 4 and 5. The remaining 18 parts do not produce any new phase portrait which was not included in the 25 previous ones. The phase portraits are basically different to each other under some algebro–geometric features related to the position of the orbits.

The phase portraits having neither limit cycle nor graphic have been denoted surrounded by parenthesis, for example (V_1^1) (in Tables 1 and 4); the phase portraits having one limit cycle have been denoted surrounded by brackets, for example $[V_{11}^5]$ (in Table 1); the phase portraits having at least one graphic have been denoted surrounded by {}, for example $\{7S_1^{23}\}$ (in Table 1).

Proof. The above two results follow from the results in the previous sections and a careful analysis of the bifurcation diagrams given in Secs. 6 and 7, in Figs. 11, 12, 13, 17, 18 and 19, the definition of the invariants I_j and their explicit values for the corresponding phase portraits. ■

We first make some observations regarding the equivalence relations used in this paper: the affine and time rescaling, C^1 and topological equivalences.

The coarsest one among these three is the topological equivalence and the finest is the affine equivalence. We can have two systems which are topologically equivalent but not C^1–equivalent. For example, we could have a system with a finite antisaddle which is a structurally stable node and in another system with a focus, the two systems being topologically equivalent but belonging to distinct C^1–equivalence classes, separated by the surface $\mathcal{S}_6$ on which the node turns into a focus.

In Table 3 (Table 6, respectively) we listed in the first column 38 parts (25 parts, respectively) with all the distinct phase portraits of Figs. 1 and 2 (Fig. 3, respectively). Corresponding to each part listed in column 1 we have in its horizontal block, all parts whose phase portraits are topologically equivalent to the phase portrait appearing in column 1 of the same horizontal block.

In the second column we have put all the parts whose systems yield topologically equivalent phase

portraits to those in the first column, but which may have some algebro–geometric features related to the position of the orbits.

In the third (respectively, fourth, and fifth) column we list all parts whose phase portraits have another antisaddle which is a focus (respectively, a node which is at a bifurcation point producing foci close to the node in perturbations, a node–focus to shorten, and a finite weak singular point). In the sixth column of Table 1 we list all phase portraits which have a triple infinite singularity with multiplicity $\binom{2}{1}$.

Whenever phase portraits appear on a horizontal block in a specific column, the listing is done according to the decreasing dimension of the parts where they appear, always placing the lower dimensions on lower lines.

9.1. Proof of the main theorem

The bifurcation diagram described in Sec. 6, plus Tables 1 and 2 of the geometrical invariants distinguishing the 38 phase portraits, plus Table 3 giving the equivalences with the remaining phase portraits lead to the proof of the main statement of Theorem 1.1. Analogously, we have the proof of Theorem 1.2, but considering the description in Sec. 7 and Tables 4, 5 and 6.

To prove statements *(d)* and *(e)* of Theorem 1.2 we recall the Main Theorem of [Vulpe, 2011] and verify that:

(i) Any representative of $4S_1^{10}$ is such that $g \neq 0$ (we may assume $g = 1$), $h > 0$, $\ell = 0$ and $m > 1/2$. Then, we have: $\mathcal{T}_4 = 0$, $\mathcal{T}_3 = 8h^2(2m - 1) \neq 0$, $\mathcal{T}_3\mathcal{F} = -8h^4(2m-1)^3 < 0$, $\mathcal{F}_1 = \mathcal{F}_2 = \mathcal{F}_3\mathcal{F}_4 = 0$, which imply that it has a center c;

(ii) Any representative of $4S_2^1$ is such that $g \neq 0$ (we may assume $g = 1$), $h > 0$, $\ell = 0$ and $m < 1/2$. Then, we have: $\mathcal{T}_4 = 0$, $\mathcal{T}_3 = 8h^2(2m - 1) \neq 0$, $\mathcal{T}_3\mathcal{F} = 8h^4(1 - 2m)^3 > 0$, $\mathcal{F}_1 = \mathcal{F}_2 = \mathcal{F}_3\mathcal{F}_4 = 0$, which imply that it has an integrable saddle $\$$.

We observe that the phase portraits $9S_2^{25}$ and $9S_3^{26}$ from family $\overline{QsnSN(A)}$ are not equivalent to the phase portrait $4.9L_1^{19}$ from family $\overline{QsnSN(B)}$ because the isolated infinite singular point has index 0 in the last phase portrait while its index is -1 and $+1$ in the first two phase portraits, respectively. Moreover, $9S_2^{25}$ and $9S_3^{26}$ are not equivalent since they are different by the invariant I_8.

However, the phase portrait P_3^{36} from family $\overline{QsnSN(A)}$ is equivalent to the phase portrait P_2^{23} from family $\overline{QsnSN(B)}$ since there are no invariant that distinguishes them. The same argument applies to prove that the phase portrait $1.2L_2^{27}$ from family $\overline{QsnSN(A)}$ is equivalent to the phase portrait $1.4L_1^{15}$ from family $\overline{QsnSN(B)}$, and this proves Corollary 1.3.

TABLE 1: Geometric classification for the subfamily $\overline{QsnSN(A)}$: the non–degenerate parts.

$$
I_1 = \left\{
\begin{array}{l}
3 \ \&\ I_2 = \left\{
\begin{array}{l}
2 \ \&\ I_3 = \left\{
\begin{array}{l}
2 \ \&\ I_4 = \left\{
\begin{array}{l}
2111 \ \&\ I_5 = \left\{ \begin{array}{l} 1\ [V_{14}^{7}], \\ 0\ (V_{12}^{6}), \end{array} \right. \\
1111 \ \&\ I_6 = \left\{ \begin{array}{l} 1\ \{4S_4^{19}\}, \\ 0\ (V_{15}^{8}), \end{array} \right.
\end{array} \right. \\
1\ (5S_3^{22}),
\end{array} \right. \\
0 \ \&\ I_3 = \left\{
\begin{array}{l}
2 \ \&\ I_4 = \left\{
\begin{array}{l}
4111 \ \&\ I_5 = \left\{ \begin{array}{l} 1\ [V_{11}^{5}], \\ 0\ (V_{9}^{4}), \end{array} \right. \\
2111 \ \&\ I_6 = \left\{ \begin{array}{l} 1\ (4S_1^{18}), \\ 0\ (V_{6}^{3}), \end{array} \right. \\
3112\ (V_3^2), \\
2120\ (V_{16}^{9}), \\
3111\ \{7S_1^{23}\},
\end{array} \right. \\
1\ (5S_2^{21}),
\end{array} \right.
\end{array} \right. \\
2 \ \&\ I_2 = \left\{
\begin{array}{l}
\infty\ \{1.2L_2^{27}\}, \\
1 \ \&\ I_3 = \left\{
\begin{array}{l}
2 \ \&\ I_4 = \left\{
\begin{array}{l}
2111 \ \&\ I_5 = \left\{ \begin{array}{l} 1\ [1S_2^{11}], \\ 0\ (1S_4^{12}), \end{array} \right. \\
1111 \ \&\ I_6 = \left\{ \begin{array}{l} 1\ \{1.4L_1^{28}\}, \\ 0\ (1S_1^{10}), \end{array} \right. \\
2110\ (1S_5^{13}),
\end{array} \right.
\end{array} \right. \\
0 \ \&\ I_3 = \left\{
\begin{array}{l}
2 \ \&\ I_4 = \left\{
\begin{array}{l}
2111 \ \&\ I_6 = \left\{ \begin{array}{l} 1\ (3.4L_1^{31}), \\ 0\ (3S_4^{17}), \end{array} \right. \\
3112\ (3S_1^{14}), \\
4111\ (3S_2^{15}), \\
2120\ (3S_3^{16}), \\
3111\ (2.3L_1^{30}),
\end{array} \right. \\
1\ (3.5L_1^{32}),
\end{array} \right.
\end{array} \right. \\
1 \ \&\ I_3 = \left\{
\begin{array}{l}
\infty\ \{P_1^{35}\}, \\
2\ (V_1^1), \\
1\ (5S_1^{20}).
\end{array} \right.
\end{array} \right.
$$

TABLE 2: Geometric classification for the subfamily $\overline{QsnSN(A)}$: the degenerate parts.

$$
I_1 = \left\{
\begin{array}{l}
1 \ \&\ I_2 = \left\{
\begin{array}{l}
1 \ \&\ I_3 = \left\{
\begin{array}{l}
\infty\ \{P_3^{36}\}, \\
2 \ \&\ I_8 = \left\{ \begin{array}{l} -1\ \{9S_2^{25}\}, \\ 1\ (9S_3^{26}), \end{array} \right. \\
1\ \{5.9L_1^{33}\},
\end{array} \right. \\
-1\ \{9S_1^{24}\},
\end{array} \right. \\
0 \ \&\ I_3 = \left\{
\begin{array}{l}
2 \ \&\ I_8 = \left\{
\begin{array}{l}
1 \ \&\ I_9 = \left\{ \begin{array}{l} 2\ \{P_4^{37}\}, \\ 1\ \{8.9L_1^{34}\}, \end{array} \right. \\
0\ \{1.9L_1^{29}\},
\end{array} \right. \\
1\ \{P_5^{38}\}.
\end{array} \right.
\end{array} \right.
$$

TABLE 3: Topological equivalences for the subfamily $\overline{QsnSN(A)}$.

Presented phase portrait	Identical under perturbations	Finite antisaddle focus	Finite antisaddle node–focus	Finite weak point	Triple infinite point
V_1^1	V_2^1				$1.3L_1^1$
V_3^2	V_4^2, V_5^2		$6S_2^2$	$2S_2^2$	
V_6^3	V_{18a}^3, V_{18b}^3 $4S_5^3$	V_7^3, V_8^3, V_{19}^3, V_{20}^3	$6S_1^3$, $6S_7^3$	$2S_1^3$, $2S_5^3$	
V_9^4		V_{10}^4	$6S_3^4$	$2S_3^4$	
V_{11}^5					
V_{12}^6		V_{13}^6	$6S_4^6$	$2S_4^6$	
V_{14}^7					
V_{15}^8	V_{21}^8	V_{17}^8, V_{22}^8	$6S_5^8$, $6S_6^8$		
V_{16}^9					
$1S_1^{10}$	$1S_6^{10}$				
$1S_2^{11}$					
$1S_4^{12}$		$1S_3^{12}$ $1.6L_1^{12}$		$1.2L_1^{12}$	
$1S_5^{13}$					
$3S_1^{14}$					
$3S_2^{15}$					
$3S_3^{16}$					
$3S_4^{17}$					
$4S_1^{18}$		$4S_2^{18}$, $4S_3^{18}$	$4.6L_1^{18}$	$2.4L_1^{18}$	
$4S_4^{19}$					
$5S_1^{20}$					
$5S_2^{21}$					
$5S_3^{22}$					
$7S_1^{23}$					
$9S_1^{24}$	$9S_4^{24}$ $4.9L_1^{24}$				
$9S_2^{25}$	$9S_5^{25}$ $4.9L_2^{25}$				
$9S_3^{26}$	$9S_6^{26}$ $4.9L_3^{26}$				
$1.2L_2^{27}$					
$1.4L_1^{28}$					
$1.9L_1^{29}$	$1.9L_2^{29}$ P_2^{29}				
$2.3L_1^{30}$					
$3.4L_1^{31}$	$3.4L_2^{31}$				
$3.5L_1^{32}$					
$5.9L_1^{33}$	$5.9L_2^{33}$				
$8.9L_1^{34}$	$8.9L_2^{34}$				
P_1^{35}					
P_3^{36}					
P_4^{37}					
P_5^{38}					

TABLE 4: Geometric classification for the subfamily $\overline{QsnSN(B)}$: the non–degenerate parts.

$$
I_1 = \left\{
\begin{array}{ll}
3 \ \& \ I_2 = \left\{
\begin{array}{ll}
2 \ \& \ I_3 = \left\{
\begin{array}{ll}
2 \ \& \ I_4 = \left\{
\begin{array}{ll}
1111 \ \& \ I_7 = \left\{
\begin{array}{l}
32 \ (V_6^4), \\
31 \ (V_7^5), \\
20 \ \{4S_1^{10}\},
\end{array}
\right. \\
1121 \ (V_3^3),
\end{array}
\right. \\
1 \ (5S_1^{11}),
\end{array}
\right. \\
0 \ \& \ I_3 = \left\{
\begin{array}{ll}
2 \ \& \ I_4 = \left\{
\begin{array}{l}
2120 \ (V_2^2), \\
1121 \ \{V_1^1\},
\end{array}
\right. \\
1 \ (5S_3^{12}),
\end{array}
\right.
\end{array}
\right. \\
2 \ \& \ I_2 = \left\{
\begin{array}{ll}
2 \ \& \ I_3 = \left\{
\begin{array}{l}
2 \ (9S_1^{13}), \\
1 \ (5.9L_1^{20}),
\end{array}
\right. \\
1 \ \& \ I_3 = \left\{
\begin{array}{ll}
\infty \ \{1.4L_1^{15}\}, \\
2 \ \& \ I_4 = \left\{
\begin{array}{l}
1120 \ (1S_2^7), \\
1111 \ (1S_1^6),
\end{array}
\right.
\end{array}
\right. \\
0 \ \& \ I_3 = \left\{
\begin{array}{l}
2 \ (9S_2^{14}), \\
1 \ (5.9L_2^{21}),
\end{array}
\right.
\end{array}
\right. \\
1 \ \& \ I_3 = \left\{
\begin{array}{ll}
\infty \ \{P_1^{22}\}, \\
2 \ \& \ I_4 = \left\{
\begin{array}{l}
2121 \ \{1S_4^9\}, \\
1111 \ \{1.4L_2^{16}\}, \\
1011 \ (1S_3^8),
\end{array}
\right. \\
1 \ \{1.5L_1^{17}\}.
\end{array}
\right.
\end{array}
\right.
$$

TABLE 5: Geometric classification for the subfamily $\overline{QsnSN(B)}$: the degenerate parts.

$$
I_1 = \left\{
\begin{array}{ll}
1 \ \& \ I_3 = \left\{
\begin{array}{l}
\infty \ \{P_2^{23}\}, \\
2 \ \{4.9L_1^{19}\},
\end{array}
\right. \\
0 \ \& \ I_{10} = \left\{
\begin{array}{l}
>< \ \{1.9L_1^{18}\}, \\
\cup \ \{P_3^{24}\}, \\
\times \ \{P_4^{25}\},
\end{array}
\right.
\end{array}
\right.
$$

TABLE 6: Topological equivalences for the subfamily $\overline{QsnSN(B)}$.

Presented phase portrait	Identical under perturbations	Finite antisaddle focus	Finite antisaddle node–focus	Finite weak point
V_1^1	V_9^1			$4S_2^1$
V_2^2				
V_3^3		V_4^3	$6S_3^3$	
V_6^4		V_5^4	$6S_1^4$	
V_7^5		V_8^5	$6S_2^5$	
$1S_1^6$				
$1S_2^7$				
$1S_3^8$	$1S_6^8$			$1.4L_3^8$
$1S_4^9$	$1S_5^9$			
$4S_1^{10}$				
$5S_1^{11}$		$5S_2^{11}$	$5.6L_1^{11}$	
$5S_3^{12}$				
$9S_1^{13}$	$9S_3^{13}$			
$9S_2^{14}$	$9S_4^{14}$			
$1.4L_1^{15}$				
$1.4L_2^{16}$				
$1.5L_1^{17}$	$1.5L_2^{17}$			
$1.9L_1^{18}$	$1.5L_3^{14}$			
$4.9L_1^{19}$	$4.9L_2^{19}$			
$5.9L_1^{20}$				
$5.9L_2^{21}$				
P_1^{22}				
P_2^{23}				
P_3^{24}				
P_4^{25}				

Acknowledgements. The first author is partially supported by a MEC/FEDER grant number MTM 2008–03437 and by a CICYT grant number 2005SGR 00550, the second author is supported by CAPES/DGU grant number BEX 9439/12–9 and the last author is partially supported by CAPES/DGU grant number 222/2010 and by FP7–PEOPLE–2012–IRSES–316338.

References

Andronov, A.A., Leontovich, E.A., Gordon, I.I. & Maier, A.G. [1973] "Qualitative theory of second–order dynamic systems." *Israel Program for Scientific Translations* (Halsted Press, A division of John Wiley & Sons, NY-Toronto, Ontario).

Artés, J.C., Kooij, R. & Llibre, J. [1998] "Structurally stable quadratic vector fields," Memoires Amer. Math. Soc., **134 (639)**.

Artés, J.C. & Llibre, J. [2013] "Structurally unstable quadratic systems of codimension 1", *Work in progress.*

Artés, J.C., Llibre, J. & Schlomiuk, D. [2006] "The geometry of quadratic differential systems with a weak focus of second order," *Internat. J. Bifur. Chaos Appl. Sci. Engrg.* **16**, 3127–3194.

Artés, J.C., Llibre, J. & Vulpe, N. [2008] "Singular points of quadratic systems: a complete classification in the coefficient space $\mathbb{R}^{12}$," *Internat. J. Bifur. Chaos Appl. Sci. Engrg.* **18**, 313–362.

Artés, J.C., Llibre, J., Schlomiuk, D. & Vulpe, N.I. [2012] "From topological to geometric equivalence in the classification of singularities at infinity for quadratic vector fields", *Rocky Mountain J. Math.* (accepted)

Artés, J.C., Rezende, A.C., & Oliveira, R.D.S. [2013] "Global phase portraits of quadratic polynomial differential systems with a semi–elemental triple node," *Internat. J. Bifur. Chaos Appl. Sci. Engrg.* **23**, 21 pp.

Bautin, N.N. [1954] "On periodic solutions of a system of differential equations," *Prikl. Mat. Meh.* **18**, 128.

Coll, B. & Llibre, J. [1988] "Limit cycles for a quadratic system with an invariant straight line and some evolution of phase portraits," *Qualitative Theory of Differential Equations, Colloq. Math. Soc. János Bolyai, Bolyai Institut, Szeged, Hungria* **53**, 111–123.

Coppel, W.A. [1966] "A survey of quadratic systems," *J. Differential Equations* **2**, 293–304.

Darboux, G. [1878] "Mémoire sur les équations différentielles algébriques du premier ordre et du premier degré (mélanges)," *Bull. Sci. Math.* **124A**, 60–96, 123–144, 151–200.

Dumortier, F., Llibre, J. & Artés, J.C. [2006] "Qualitative Theory of Planar Differential Systems," *Universitext, Springer–Verlag, New York–Berlin.*

Dumortier, F., Roussarie, R. & Rousseau, C. [1994] "Hilbert's 16th problem for quadratic vector fields," *J. Differential Equations* **110**, 66–133.

Fulton, W. [1969] "Algebraic curves. An introduction to Algebraic Geometry," *W.A. Benjamin, Inc.*, New York.

González, E.A. [1969] "Generic properties of polynomial vector fields at infinity," *Trans. Amer. Math. Soc.* **143**, 201–222.

Hartshorne, R. [1977] "Algebraic geometry," *Graduate Texts in Math.* **52**, Springer.

Hilbert, D. [1900] "Mathematische probleme", *In Nachr. Ges. Wiss., editor Second Internat. Congress Math. Paris, 1900*, 253–297. Göttingen Math.–Phys. Kl.

Hilbert, D. [1902] "Mathematical problems," *Bull. Amer. Math. Soc.* **8**, 437–479.

Llibre, J. & Schlomiuk, D. [2004] "The geometry of quadratic differential systems with a weak focus of third order," *Canad. J. Math.* **56**, 310–343.

Roussarie, R. & Schlomiuk, D. [2002] "On the geometric structure of the class of planar quadratic differential systems," *Qual. Theory Dyn. Syst.* **3**, 93–122.

Schlomiuk, D. & Pal, J. [2001] "On the geometry in the neighborhood of infinity of quadratic differential systems with a weak focus," *Qual. Theory Dyn. Syst.* **2**, 1–43.

Schlomiuk, D. & Vulpe, N.I. [2005] "Geometry of quadratic differential systems in the neighborhood of the infinity," *J. Differential Equations* **215**, 357–400.

Vulpe, N.I. [2011] "Characterization of the finite weak singularities of quadratic systems via invariant theory," *Nonlinear Anal.* **74**, 6553–6582.

Ye, Y.Q. *et al.* [1986] "Theory of limit cycles," *Trans. of Mathematical Monographs*, **66**. Amer. Math. Soc., Providence, RI, 2 edition.